Virus glycoprotein nanodisc platform for vaccine design

Kimmo Rantalainen[1,2,3], Alessia Liguori[1,2,3], Gabriel Ozorowski[3,4], Claudia Flynn[1,2,3], Jon M. Steichen[1,2,3], Olivia Swanson[1,2,3,4], Patrick J. Madden[3,5], Sabyasachi Baboo[4], Swastik Phulera[4], Anant Gharpure[4], Danny Lu[1,2,3], Oleksandr Kalyuzhniy[1,2,3], Patrick Skog[1,2,3], Sierra Terada[1,2,3], Monolina Shil[3,5], Jolene K. Diedrich[4], Erik Georgeson[1,2,3], Ryan Tingle[1,2,3], Saman Eskandarzadeh[1,2,3], Wen-Hsin Lee[4], Nushin Alavi[1,2,3], Diana Goodwin[1,2,3], Michael Kubitz[1,2,3], Sonya Amirzehni[1,2,3], Sunny Himansu[6], Devin Sok[1,2,3], Jeong Hyun Lee[1,2,3], John R. Yates III[4], James C. Paulson[1,3,6], Shane Crotty[3,5,7], Torben Schiffner[1,2,3,8,*], Andrew B. Ward[3,4,*], William R. Schief[1,2,3,6,*]

Affiliations

[1] Department of Immunology and Microbiology, The Scripps Research Institute, La Jolla, CA, USA.

[2] IAVI Neutralizing Antibody Center, The Scripps Research Institute, La Jolla, CA, USA.

[3] Consortium for HIV/AIDS Vaccine Development (CHAVD), The Scripps Research Institute, La Jolla, CA, USA.

[4] Department of Integrative Structural and Computational Biology, The Scripps Research Institute, La Jolla, CA 92037, USA.

[5] Center for Vaccine Innovation, La Jolla Institute for Immunology, La Jolla, CA 92037, USA.

[6] Moderna Inc., Cambridge, MA, 02139, USA.

[7] Division of Infectious Diseases, Department of Medicine, University of California San Diego, La Jolla, CA 92037, USA.

[8] Institute for Drug Discovery, Leipzig University Medical Faculty, Leipzig, 04103, Germany

*Corresponding authors. Email: torbens@scripps.edu (T.S.), andrew@scripps.edu (A.B.W.), or schief@scripps.edu (W.R.S.)

Abstract

Transmembrane glycoproteins of enveloped viruses are the targets of neutralizing antibodies and essential vaccine antigens. mRNA-LNP technology allows in situ production of transmembrane glycoproteins upon immunization, but biophysical characterization of transmembrane antigens and in vitro analysis of post-immunization antibody responses typically rely on soluble proteins. Here, we present a methodological platform for assembling transmembrane glycoprotein vaccine candidates into lipid nanodiscs. We demonstrate the utility of the nanodiscs in HIV membrane proximal external region (MPER)-targeting vaccine development by binding assays using surface plasmon resonance (SPR), ex vivo B cell sorting with fluorescence-activated cell sorting (FACS), and by determining the structure of a prototypical HIV MPER-targeting immunogen nanodisc in complex with three broadly neutralizing antibodies (bnAbs), including the MPER bnAb 10E8, to 3.5 Å by cryogenic electron microscopy (cryo-EM), providing a template for structure-based immunogen design for MPER. Overall, the platform offers a tool for accelerating the development of next-generation viral vaccines.

Summary

In the past two decades, nanodiscs have emerged as means to encapsulate transmembrane proteins into a stable and more native-like environment. In most cases, proteins are extracted from the membrane by detergent solubilization and then assembled into a nanodisc by removal of the detergent in presence of lipid molecules and a scaffold protein. Since the first apolipoprotein-derived membrane scaffold proteins (MSPs) were introduced, several variations and alternative scaffolds have been described, allowing for a variety of disc sizes and versatile experimental approaches[1-5]. Structural studies of membrane proteins have perhaps benefitted the most from nanodiscs, resulting in important advances in understanding of membrane protein structure-function relationship[6, 7]. They have also been used successfully in a variety of functional and biophysical approaches such as surface plasmon resonance (SPR)[8-10].

Viral glycoproteins of enveloped viruses are membrane proteins and essential targets for vaccine development. Structure-based vaccine design was an integral part of the successful COVID-19 vaccine development[11-13], and a significant portion of the groundwork stemmed from decades of HIV vaccine development[14]. Structure-based methods, combined with rapidly advancing computational protein design approaches and mRNA lipid nanoparticle (mRNA-LNP)

technology, are now revolutionizing iterative vaccine development[15, 16]. Immunogen delivery by mRNA-LNP expands the available immunogens to more native-like constructs that may contain the membrane-proximal epitopes such as the recently developed cleavage independent NFL trimers expressing HIV Env[17] and the MD39.3 gp151 Env trimer used in the HVTN302 clinical trial (NCT05217641), but recombinant transmembrane glycoprotein production for biophysical characterization of the immunogens remains challenging. In most studies, membrane proteins are truncated before the transmembrane domain to obtain soluble ectodomains with higher expression levels and easier handling and applicability in downstream analytical methods. The regions excluded typically include the membrane-proximal external region (MPER), transmembrane domain (TM), and intracellular C-terminal domain (CT). In influenza HA, the anchor region analogous to HIV MPER joins the ectodomain as flexible linkers to three transmembrane helices and allows the trimer to tilt in relation to bilayer surface[18]. Both Env MPER and HA anchor have highly conserved epitopes for neutralizing antibodies (nAbs) making them attractive targets for vaccine development[19-23]. Significant progress in MPER targeted HIV vaccine development has been made recently with peptide-liposome formulations showing induction of heterologous neutralizing antibody B cell lineages in humans, and with mRNA delivered germline-targeting (GT) epitope scaffold efficiently inducing antibody precursors in non-human primates (NHPs) and mice[24, 25]. Analysis of antibodies elicited by these vaccines as well as further immunogen development would benefit from inclusion of the full epitope in recombinantly expressed proteins. For example, recombinant proteins matching the transmembrane immunogens delivered as mRNA are required for accurate immunogen assessment in iterative vaccine design methods, such as SPR and structural studies. Importantly, transmembrane versions of Env may also be required for more accurate representations of the glycan shield, as many neutralizing antibodies bind specifically to glycans, and glycoproteins expressed as transmembrane proteins have been shown to have glycan shield compositions closer to the native glycan shield[26-28].

Some uses of nanodiscs to support vaccine development have been demonstrated, particularly in efforts to characterize the structures of HIV MPER-targeting HIV antibody epitopes and transmembrane domains of virus glycoproteins in their native membrane bilayer environment[29-33]. The nanodisc assembly platform presented here provides the reproducibility, scalability, and accurate replication of the vaccine candidate properties that enable routine use of transmembrane viral glycoproteins in key methods employed in iterative, rational vaccine design.

94 We demonstrate use of nanodiscs to measure antibody affinities by SPR, as FACS probes to sort
95 antigen-specific B cells from mouse and non-human primate (NHP) immunization experiments,
96 and for solving the cryo-EM structure of a prototype HIV boost vaccine candidate in complex with
97 three broadly neutralizing antibodies (bnAbs) that target distinct sites of vulnerability on the HIV
98 Env surface. We highlight the benefits of the approach by reporting the structure of the entire
99 protein epitope of an HIV MPER-targeting bnAb 10E8. Finally, we show the adaptability of the
100 platform to other glycoproteins by assembling engineered Ebola virus glycoprotein in nanodiscs
101 using identical conditions to HIV Env.
102
103 **Results**
104 **Glycoprotein Nanodisc Assembly and Analysis Workflow**
105 We set to establish a workflow that provides material suitable for methods commonly used in
106 rational, iterative vaccine design (Fig. 1). The workflow was set up using the engineered and highly
107 expressing HIV Env clone BG505 MD39.3 gp151[34,35] that is currently being tested in a phase 1
108 clinical trial HVTN 302 (NCT05217641). A linker, followed by an HRV3C protease cleavage site
109 and a strep tag was added to the intracellular C-terminus, leading to a nanodisc assembly construct
110 base that will hereon be referred to as Env gp151 ND (Fig. 2a-b). This construct was then used to
111 optimize the throughput and reproducibility of nanodisc production, leading to a standardized
112 workflow (Fig. 2c). In short, transmembrane glycoproteins (GPs) were expressed on the surface
113 of human FreeStyle 293-F cells, followed by detergent solubilization with TX-100-containing
114 buffer. As the transmembrane domain of viral glycoproteins is composed of only three helices –
115 one per protomer – detergent solubilization by TX-100 was not expected to disturb the quaternary
116 structure of the engineered GP trimer as indicated by the binding of structure specific antibodies
117 to extracted GPs[27, 28]. The detergent-solubilized glycoprotein was then assembled into nanodiscs
118 using the MSP1D1 scaffold with or without a biotin tag. While a variety of scaffold proteins are
119 available, we opted to reduce variables and focused on using the standard MSP1D1 scaffold for
120 all purposes. The developed "batch assembly" approach, resembling previously described "on-
121 column"[36] and "on-bead"[37] methods, facilitated reproducibility and efficient assembly while GPs
122 remained bound to the matrix. Empty nanodiscs for control experiments were produced by
123 omitting GP in the assembly step and using His-tag of the scaffold protein with NiNTA affinity
124 purification prior to SEC. Utilizing this workflow, up to 12 samples were routinely processed

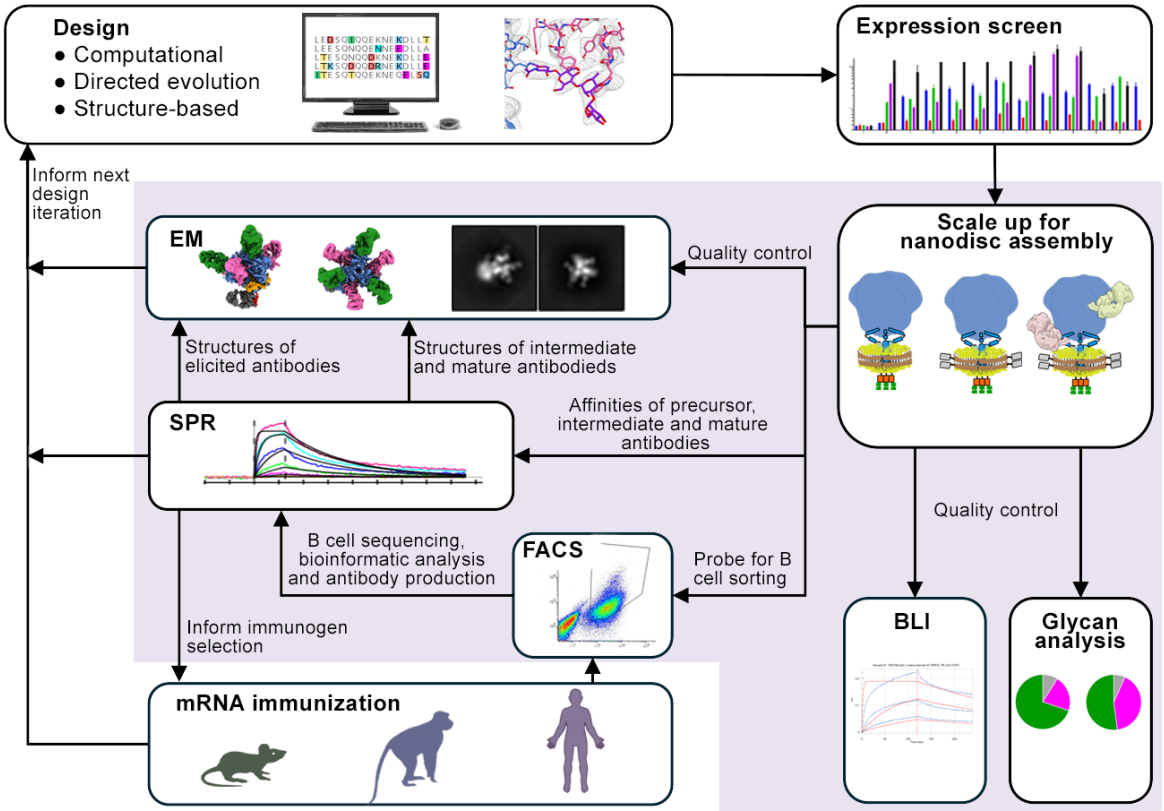

Figure 1. Nanodisc use in different steps in iterative rational vaccine design. Analytical methods that can directly use nanodiscs as sample material are highlighted.

simultaneously in five days from transfection to purified nanodisc. One liter of cells yielded approximately 100 to 700 µg of pure GP nanodiscs, which was sufficient for one to three endpoint assays. For example, a single production batch produced an EBOV GP nanodiscs, an HIV Env nanodisc-Fab complex for cryo-EM structural studies, and eight FACS probes for B cell sorting. Final GP nanodisc preparations were stable for at least three months at +4°C based on absorbance at 280 nm, presence of trimeric GP in nanodisc in negative stain (ns) EM 2D class averages, and activity in SPR analysis (Fig. 3 b).

The workflow was then piloted in an immunogen development project aiming to increase the affinity of MPER targeting antibody 10E8 and therefore guiding immune responses to MPER domain. In the native membrane context, the C-terminal MPER helix that is targeted by the heavy chain complementarity determining region 3 (CDRH3) of 10E8 is sterically occluded (Fig 2b) and one of the design goals was to improve the MPER access. To this end, N-linked glycosylation sites at positions N88, N618, and N625 (HxB2 numbering) adjacent to the epitope were removed at the

base of the trimer. An additional R696S mutation that improved 10E8 binding while maintaining trimeric Env conformation was discovered by mammalian surface display library screening. Earlier structural analysis indicated that R696 resides at the intersection of the three transmembrane helices[29, 38]; therefore, this mutation was predicted to disrupt helix interactions and further open the trimer base. The resulting construct will be referred to as Env gp151 MPER ND. A negative control for MPER antibody binding and a KO FACS probe for epitope-specific B cell sorting, designated as Env gp151 MPER-KO ND, was also generated (Fig. 2a). This construct included MPER mutations W672A, F673R, T676R, N677I, L679M, W680E, Y681W, and W683D, which were previously reported to collectively prevent the binding of MPER-targeting antibodies while preserving the overall trimeric structure of Env and other bnAb epitopes[24], or screened for this study to improve the expression construct. Prototypical Ebola GP immunogen EBOV GP Mayinga ND was based on a construct with trimer stabilizing mutations T577P and K588F[39], to which native EBOV GP TM domain and the same intracellular elements as in the HIV Env constructs were added. Assembled nanodiscs generally exhibited broad peaks in SEC spectra indicative of extensive glycosylation and variation in hydrodynamic radius that may result from positional heterogeneity of Env in the disc, and >95% purity and bands of the expected molecular weight as examined by SDS-PAGE (Supplementary Fig. 1a-b). Ns EM 2D class averages revealed features typical of nanodiscs with trimeric GP with or without Fabs (Supplementary Fig. 4a). In addition to the MPER targeting immunogen constructs and EBOV GP Mayinga ND, a germline-targeting HIV vaccine candidate N332-GT5 gp151[40, 41] was assembled into nanodiscs using the standardized workflow to test general applicability (Supplementary Fig. 2a). Mass spectrometric glycan analysis using the DeGlyPHER method[42] was done prior to and after nanodisc assembly to ascertain site-specific glycan occupancy and processivity of Env constructs. This analysis confirmed the presence of all expected glycans as well as a high proportion of complex glycans in transmembrane constructs characteristic of native, transmembrane HIV Env (Supplementary Fig. 1c). Germline-targeting immunogen N332-GT5 showed a higher proportion of complex type glycans in soluble version of the immunogen, matching closely the glycan composition of the transmembrane version. All transmembrane Envs showed higher glycan occupancy in gp41 subunit.

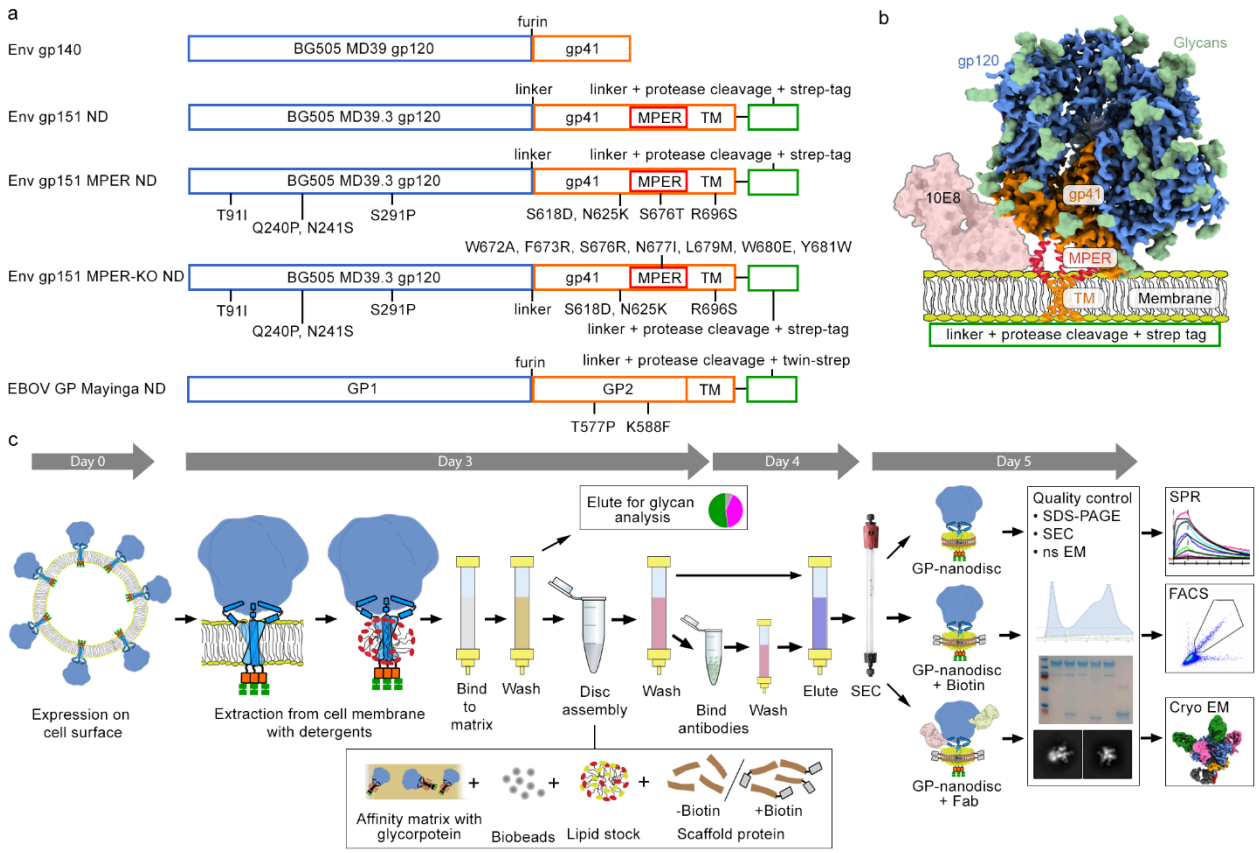

Figure 2. HIV Env constructs used for method development and general overview of the nanodisc assembly workflow. a) Naming and gene organization of the glycoprotein constructs used for nanodisc assembly. Introduced mutations and intracellular elements are indicated. ND refers to constructs made for nanodisc platform. b) Schematic overview of HIV Env constructs and MPER targeting antibody 10E8 binding. c) Key steps of the 5-day workflow for glycoprotein nanodisc assembly. Glycoprotein was extracted with detergent from cell surface and bound to affinity matrix. Disc assembly was performed "in-batch" while bound to affinity purification matrix. Assembled discs were then eluted for final SEC polishing purification, followed by quality control steps before subjecting to final analytical methods (SPR, FACS, cryo-EM).

GP nanodisc binding kinetics to antibodies measured by SPR

SPR is an essential method in iterative vaccine design that measures antibody affinities to engineered immunogens, assessing the effect of the designed features as well as affinities of antibodies induced by vaccination (Fig 1). We set to establish scalable and reproducible conditions for measuring antibody binding kinetics against transmembrane GPs in nanodiscs in three distinct SPR modalities (Fig. 3a). Modality A utilized an anti-affinity tag capture strategy in which anti-strep-tag antibody was covalently immobilized on the chip surface, glycoprotein nanodiscs were captured using the intracellular strep tag, and Fab analytes were employed to study monovalent

interactions. Modality B employed a low surface density IgG capture strategy, in which anti-human IgG capture antibody was first covalently immobilized, and glycoprotein-specific IgG ligands were captured at reduced capture time to limit the ligand density. Glycoprotein nanodiscs were then injected as analytes. In modality C, nanodisc capture is followed by IgG flow as analyte instead of Fabs, allowing a high throughput scouting approach with low nanodisc sample consumption but with reduced kD accuracy due to increased bivalent interaction. Establishing these three modalities for nanodisc GPs allowed flexibility in experiment design based on the need in iterative vaccine development step and sample availability.

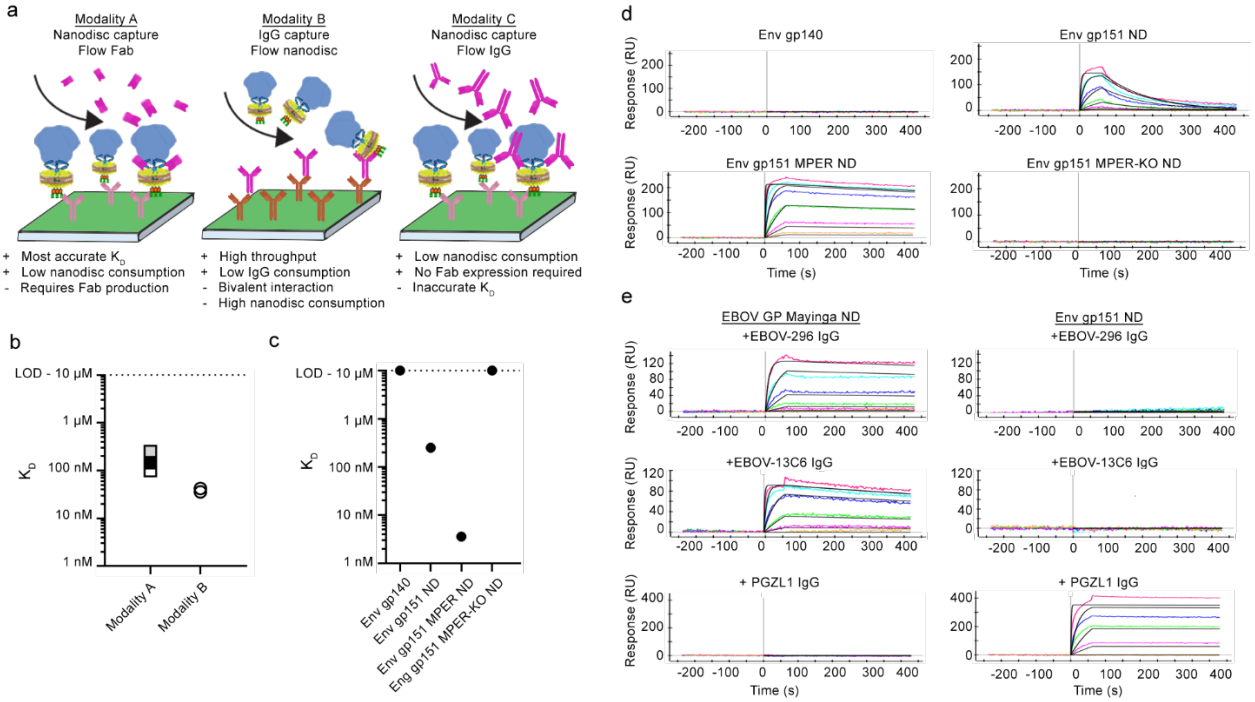

Figure 3. Different SPR modalities and kinetic analyses of GP nanodiscs. a) Schematic illustrations of three SPR modalities used throughout the study and their strengths and weaknesses. b) Affinity of MPER targeting 10E8 antibody to Env gp151 ND as measured with modalities A and B. Affinities with modality A were measured after storing the sample either 1 week (white), 1 month (grey) or 3 months (black) at 4°C. c) Affinity of 10E8 against Env constructs using modality A. d) SPR data presented in (c), showing increase in affinity originating from reduced off-rate in Env gp151 MPER ND. e) Modality C was used to scout Ebola specific EBOV-296 and EBOV-13C6 IgG epitope accessibility in EBOV GP nanodiscs. Data shows binding of two anti -Ebola antibodies targeting the glycan cap (EBOV-296 and 13C6). Env gp151 ND and anti-HIV MPER antibody PGZL1 were used as a negative controls.

211 Next, we used the GP nanodisc SPR modalities to establish baseline kinetics for
212 neutralizing and non-neutralizing monoclonal HIV Env antibodies spanning diverse epitopes (Fig.
213 3b-d, Supplementary Fig. 2b-d). Modality A measured 250 – 100 nM affinity for 10E8 to Env
214 gp151 ND design base construct (Fig. 3b) and slightly higher affinity of 36 – 42 nM using modality
215 B, indicating that the low-density capture reduced but did not eliminate the avidity effects of
216 Modality B. Using modality A, we observed 70-fold increase in 10E8 affinity (250 nM vs 3.6 nM)
217 to Env gp151 MPER ND as a result of removal of the MPER epitope-proximal glycans and the
218 mutation R696S in TM (Fig. 3c). Kinetic analysis indicated that the improved affinity in the
219 engineered immunogen was primarily attributed to a decreased off-rate (8.1×10^{-3} s^{-1} for Env
220 gp151 ND vs 3.5×10^{-4} s^{-1} for Env gp151 MPER ND. Fig. 3d). Incorporation of MPER-KO
221 mutations completely abrogated 10E8 binding. Additional MPER targeting bnAbs and bnAbs
222 targeting other epitopes on the surface of Env were also tested for more comprehensive antigenic
223 profiling. Expectedly, this confirmed binding of MPER targeting antibodies to Env gp151 ND and
224 no binding to Env gp140 (Supplementary Fig. 2b), and similar affinities of non-MPER bNabs to
225 soluble Env gp140 and Env gp151 ND (Supplementary Fig. 2c), with reduced or absent binding
226 of non-neutralizing antibodies RM19R and RM20A3 to Env gp151 ND as compared to Env gp140
227 (Supplementary Fig 2d). These two antibodies target the base of the trimer, which is exposed in
228 Env gp140, whereas in Env gp151 ND access is presumably restricted by MPER and TM domains
229 as well as the lipid surface of the nanodisc. Finally, we employed modality C to confirm the
230 binding of two Ebola GP glycan cap specific antibodies EBOV-296 and 13C6 to EBOV GP
231 nanodiscs (Fig. 3e). Collectively, these data demonstrate that GP nanodiscs and SPR can be used
232 to characterize the antigenic landscape of the designed transmembrane immunogen, inform
233 immunogen selection for in vivo studies, identify suitable complexes for structural studies by cryo-
234 EM and support GP nanodisc use as B cell sorting probes in FACS (Fig 1).
235

236 **FACS sorting of B Cells from immunized animal models using nanodisc GP probes**

237 Single B cell sorting and sequencing is routinely used to analyze B cell responses induced in vivo.
238 Typically, biotin-tagged variants of the immunogen are used with streptavidin. This allows
239 conjugation with multiple fluorochromes to increase selection specificity. By including a matching
240 sorting probe with KO mutations in the targeted epitope, epitope-specific responses can be
241 separated from off-target responses against unrelated epitopes. Soluble GP protein constructs

242 solely consisting of the ectodomain are most often used as antigenic baits. For immunization
243 studies where membrane-proximal epitopes are of interest, such as the HIV MPER, soluble probes
244 would not be able to extract all appropriate responses to the targeted epitope due to several
245 challenges which include 1) the hydrophobicity of the epitope regions which make bait production
246 challenging, 2) non-native or incomplete structural conformation of the epitope in shorter peptide
247 representations of the antigen, 3) missing lipid membrane components which constitute a portion
248 of the native epitope. Here, we used biotinylated MSP1D1 scaffold to generate nanodisc GP FACS
249 probes. We first tested Env gp151 ND probe binding to FACS compensation beads conjugated to
250 10E8, DH511 or BG18 bnAbs (Fig. 4a). Background signal was measured as binding to either
251 MSP1D1 scaffold protein alone, empty nanodisc assembled with DOPC lipids, or to empty
252 nanodisc with mixture of neutral and charged lipids. Env gp151 ND exhibited substantially higher
253 signal compared to controls, confirming that adequate separation from background signal can be
254 detected. We detected no binding with any of the tested probes to unimmunized C57BL/6 (B6)
255 mouse splenocytes, and a strong signal against engineered Ramos cells expressing the bnAb
256 VRC01 as its B cell receptor (BCR) [43]. This data indicated that Env nanodisc probes were suitable
257 for detection of B cells from mice by flow cytometry that specifically target Env.

258 We then proceeded with a pilot immunization experiment in mice to explore if vaccine
259 elicited antigen-specific B cells could be identified using Env nanodiscs probes. We utilized
260 transgenic mice expressing the human D3-3 and J_H6 genes that allow mice to express long
261 HCDR3s, including HCDR3 precursors of HIV MPER bnAbs 10E8, DH511 and LN01[24]. Mice
262 were intramuscularly injected with 10 µg of mRNA-LNPs encoding HIV Env gp151 MPER ND
263 construct. Animals were sacrificed, and spleens and lymph nodes were harvested 6 weeks post
264 immunization. B cells were stained with immunogen-matched (WT) nanodisc probes on two
265 distinct fluorophores and Env gp151 MPER-KO ND nanodisc probe with KO mutations in the
266 MPER to identify MPER-specific cells (Fig. 4b and Supplementary Fig. 3). Among class-switched
267 memory B cells (defined as $CD19^+IgD^-IgM^-$), 0.7% of cells were determined to be antigen-
268 specific, compared to 0.15% within the IgD^+IgM^+ naïve B cell population (Fig. 4c). This ~4.7-fold
269 increase was statistically significant (p=0.0177), indicating that the mRNA immunization elicited
270 HIV Env gp151 MPER -specific responses that could be detected by Env nanodisc probes. The
271 proportion of WT Env nanodisc-binding B cells that selectively bound to the 10E8 epitope (%KO^-
272 of WT^{++} B cells) was indistinguishable between the naïve and memory B cell compartments,

suggesting that the immunogen did not elicit MPER-specific responses, and that further engineering or inclusion of a prior priming immunogen in the immunization regimen would be required to achieve that capacity.

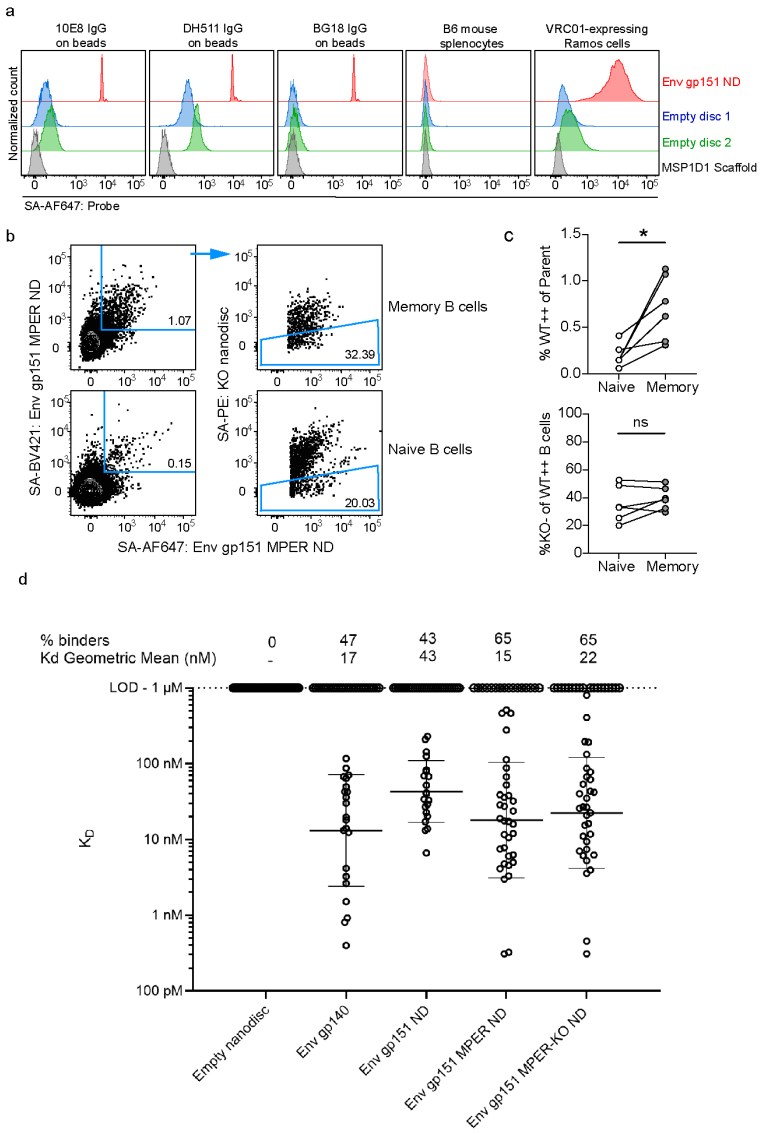

Figure 4. HIV Env nanodisc FACS probe validation and pilot use in pre-clinical mouse model. a) Nanodiscs were tested for binding to HIV MPER bnAbs 10E8 and DH511 and gp120-specific bnAb BG18 coupled to FACS compensation beads, B6 mouse splenocytes were used as negative control cells, and VRC01 expressing Ramos cells as positive control cells. Empty nanodiscs were assembled with either DOPC lipids (blue) or a mixture of neutral and charged lipids (green). b) Memory ($CD19^{+}IgM^{-}IgD^{-}$) and naïve ($CD19^{+}IgM^{+}IgD^{+}$) B cells from mice 6 weeks after immunization with mRNA-LNPs encoding Env gp151 MPER ND nanodisc were analyzed by flow cytometry. Antigen-specific (Env gp151 MPER ND^{++}) and epitope-specific (KO^{-}) B cells were detected using immunogen-matched WT and 10E8-epitope KO nanodisc probes and WT $nanodisc^{++}$ cells were sorted for BCR sequencing. The complete gating strategy is shown in

287 supplementary Fig. 3. c) Percent antigen-specific memory B cells in the naïve vs. memory
288 compartments of each immunized mouse (top), and proportion of 10E8 epitope-specific (KO^-)
289 cells within each antigen-specific population. Paired t-test, *$p < 0.05$, ns: $p > 0.05$. d) Sorted cells
290 were sequenced and selected antibodies were purified for affinity measurement by SPR using
291 modality B.
292
293 Antigen-specific (WT^{++}) mouse memory B cells were sorted and their BCRs sequenced to
294 assess the robustness of nanodisc probes in the selection of antigen-specific BCRs. Eight
295 antibodies from each animal were randomly selected for monoclonal antibody production. An
296 additional 12 antibodies with long (>=19 AA) CDRH3s were selected and duplicate antibodies
297 (containing identical heavy- and light chains) were removed, resulting in 54 total antibodies. Genes
298 encoding these antibodies were synthesized and 49 out of 54 antibodies were successfully
299 expressed, purified and used in SPR modality B to measure affinities against Env nanodiscs (Fig.
300 4d). At 1 μM analyte concentration, no non-specific responses to empty nanodiscs were detected.
301 Out of the tested antibodies, 47% bound to soluble gp140 matching the immunogen ectodomain
302 and 65% to Env gp151 MPER ND or Env gp151 MPER-KO ND. Considerable binding to
303 ectodomain, similar binding to MPER targeting immunogen and its MPER KO version and overall
304 similar geometric mean affinity to tested Env nanodiscs provided evidence that the elicited
305 antibodies were not targeting the MPER peptide but bound to the exposed base epitope or other
306 off-target epitopes. Nevertheless, using the nanodiscs as FACS sorting probes and in SPR, we were
307 able to sort and measure affinities of several antibodies that were specific to the transmembrane
308 Env gp151 version (e.g. Ab_38, Ab_48, Ab_79. Supplementary Fig. 3b).
309 Non-human primates (NHPs) are an important model for late-stage pre-clinical vaccine
310 development and are often used as final validation before clinical trials. Rhesus macaques, like
311 humans, have extensive genetic diversity within the immunoglobulin loci and are also capable of
312 making long CDRH3s [44-46]. To test whether nanodisc-based FACS tetramer probes could be
313 successfully used in RMs, experiments were carried out using PBMCs from animals immunized
314 previously with soluble Env MD39[47]. PBMCs were stained with the nanodisc probes to determine
315 whether there was substantial background binding to the lipid component of the nanodisc probes.
316 Pre-immunization PBMCs showed low background binding of IgD^- memory B cells to nanodisc,
317 while PBMCs from 2-weeks post an MD39 booster immunization showed high binding to the
318 nanodisc probes (Fig. 5a). Next, the nanodisc probes were compared directly to soluble Env gp140
319 protein probes in RMs that had been immunized with MD39.3 gp151 mRNA (matching Env gp151

320 ND sequence) 4-weeks prior[48]. Across two animals there were no differences in the frequency of
321 tetramer^{++} cells between the Env gp151 ND nanodisc and Env gp140 soluble protein probes (Fig.
322 5b). Taken together these data show that nanodiscs bearing stabilized HIV Env constructs can be
323 deployed as tetramer probes for the evaluation of pre-clinical HIV B cell responses in NHPs.
324

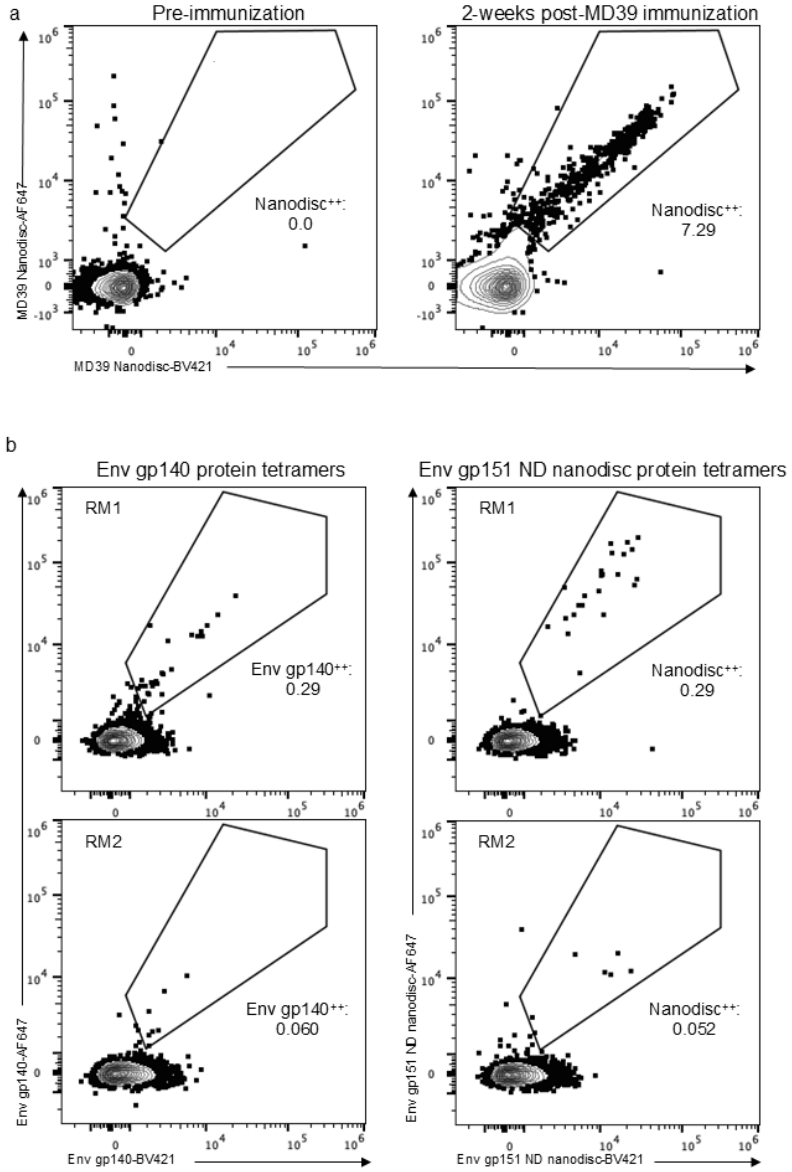

325

326 **Figure 5.** HIV Env nanodisc probe validation for sorting NHP cells. a) Flow cytometry plots
327 showing CD20^{+}IgD^{-} memory B cells stained with Env gp151 ND nanodisc on two different
328 fluorophores. Pre-immunization and 2-weeks post-immunization PBMCs from the same RM are
329 shown and the frequency of Nanodisc^{++} cells of IgD^{-} cells is listed. b) Flow cytometry plots
330 showing CD20^{+}IgG^{+} memory B cells stained with either soluble Env gp140 protein or Env gp151
331 ND nanodisc on two different fluorophores. PBMCs from two different RMs 4-weeks post mRNA

332 Env gp151 immunization were split and stained with Env gp140 protein tetramers (left column)
333 or matching nanodisc Env gp151 ND tetramers (right column). The frequency of tetramer^{++} cells
334 of IgG^{+} cells is listed for each plot.
335

336 **GP nanodiscs in cryo-EM structural studies**

337 To demonstrate how structural studies of nanodisc GPs can inform vaccine design, we set
338 out to solve the structure of prototype MPER vaccine candidate Env gp151 MPER ND in complex
339 with 10E8 antibody by cryo-EM. We included two other HIV bnAbs: VRC01, which recognize
340 the CD4 binding site, and BG18, which targets the N332 glycan supersite. This antibody cocktail
341 complex serves three purposes: First, the added Fabs improve the orientation distribution of
342 particles on cryo-EM grids. Second, they will stabilize the trimer and prevent protomers from
343 dissociating. Lastly, a functional HIV vaccine will likely require elicitation of bnAbs targeting
344 several sites to achieve sterilizing immunity. A trimer boost would therefore benefit from being
345 able to engage three or more sites (i.e. N332, CD4 and MPER) in a single immunogen. The high-
346 resolution structure of the 10E8 epitope has thus far been resolved only with x-ray crystallography
347 and in complex with MPER peptide alone[49-52]. From our cryo-EM data we produced two
348 reconstructions: the complex with two 10E8 Fabs at 4.3 Å, and the complex with a single 10E8
349 Fab at 3.5 Å resolution, which enable atomic level interpretation. We noted that while 10E8,
350 VRC01 and BG18 were all added at the same step after the nanodisc batch assembly at ~10x molar
351 excess, all VRC01 and BG18 sites were occupied but 10E8 binding site was partially
352 underoccupied in all reconstructions, suggesting steric hinderance of the MPER epitope with
353 increasing 10E8 occupancy (Fig. 6a-c). In all reconstructions, 10E8 is wedged between the Env
354 ectodomain and nanodisc lipid bilayer. MPER antibody induced Env tilt angle was evaluated by
355 aligning the low pass filtered maps to the nanodisc representing the bilayer plane. A single 10E8
356 Fab appears to be accommodated with minimal Env tilting while binding of a second 10E8 Fab
357 pushes Env into a more tilted position (Fig. 6b). Unlike in our previous WT Env AMC011 nanodisc
358 cryo-EM reconstruction, density for the TM domain remained undetected, presumably due to the
359 R696S mutation disrupting the stabilizing connection point of the three helices in the middle of
360 the bilayer[29]. The single 10E8 class was subjected to 3D variability analysis (3DVA), which
361 revealed distinct conformations of the MPER helix with ~30° lateral twist of the Fab in conjunction
362 with an apparent dislocation of the adjacent protomer (Supplementary Fig. 4c-d. Supplementary
363 video 1).

364 Using the model of Env gp151 MPER ND complex, we were able to resolve novel
365 structural details of the 10E8 epitope including a binding pocket for 10E8 antibody framework
366 region 3 (FRH3), formed by Env gp120 and gp41 subunits (Fig. 6d, inset 5). We identified 14 AA
367 in 10E8 contacting the C -terminus of gp120, helices α6 – α8 of gp41 in protomer 1, and L660 of
368 gp41 in protomer 2. These contacts are either in the binding pocket or in the helices forming a
369 collar around the termini of gp120. Strikingly, this binding pocket appeared to be targeted by the
370 CDRH3 of another HIV bnAb 3BC315, that was shown to accelerate trimer dissociation[53]. To
371 confirm this similarity in engaging the binding pocket, we solved the cryo-EM structure of Env
372 gp140 (BG505 MD39.3) in complex with BG18, VRC01 and 3BC315 Fabs to 3.1 Å resolution
373 (Fig 6f, Supplemental Fig. 4f-g). 3BC315 engages the binding pocket mainly with H100A, G100B
374 and Y100E at the tip of the CDRH3. In 10E8, the interaction is driven by I75, S74 and N76 of
375 FRH3 (Fig 6d, inset 5). The observed similarity of the binding pocket engagement led us to propose
376 that these antibodies may share a common mechanism for trimer destabilization. As part of the
377 binding pocket, both antibodies contact W623 in gp41 (Fig 6d, inset 5 and 6f), which is >99%
378 conserved across >5,000 diverse HIV strains from the LANL database (http://www.hiv.lanl.gov),
379 and has previously been shown to be part of a tryptophan clasp contributing to stabilizing four-
380 helix collar around the termini of gp120[54]. Engaging the binding pocket leads to widening of the
381 gp41 protomer-protomer gap (Fig. 6g), which would eventually lead to destabilization of the
382 contacts in the collar around the termini of gp120 and premature triggering of the fusion peptide.
383 This would normally occur during virus entry associated Env rearrangements that follow CD4
384 receptor binding. Another novel structural feature of the 10E8 antibody was the dynamic
385 remodeling of the N-terminal MPER helix, most likely driven by interactions with CDRH1 (D30,
386 N31 and W33) and CDRH2 (G52C, G53, G54, W55. Fig. 6d-e. Supplementary video 1). Root
387 mean square deviation (RMSD) of this CDRH1 and CDRH2 10E8 paratope region is 1.52 Å
388 compared to a published x-ray structure of 10E8 Fab in complex with a gp41 peptide (PDB 4G6F),
389 indicating that epitope presentation in a more native context recapitulates interactions more
390 faithfully than epitope peptide alone. In contrast, the RMSD of FRH3 between the nanodisc cryo-
391 EM complex and peptide-bound crystal structure is 0.46 Å. While the 10E8 crystal structure fit
392 well into the cryo-EM map (Supplementary Fig. 4e), we calculated an RMSD of 9.59 Å of the
393 entire MPER domain between the two structures, from the N-terminal portion of the MPER that
394 is connected to the rest of the ectodomain in the nanodisc Env cryo-EM structure. Taken together,

the comparison to previous crystal structures of 10E8 shows that native membrane environment of Env is required for complete structural characterization of the MPER targeting antibody. Observations of the native, dynamic binding mode of an MPER antibody, and structural information of the entire side chain contact network will inform the development of next-generation MPER targeting vaccines.

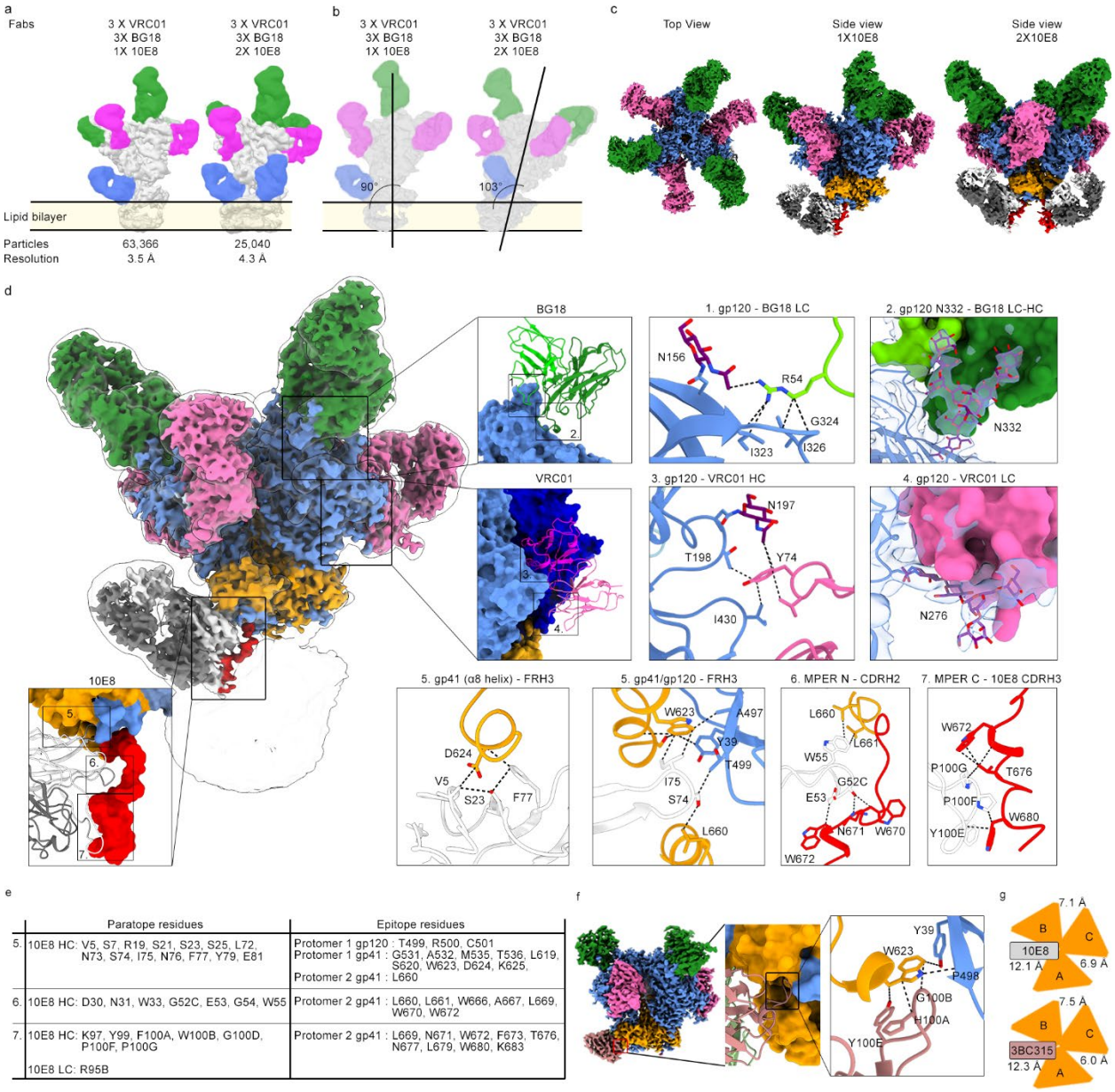

	Paratope residues	Epitope residues
5.	10E8 HC: V5, S7, R19, S21, S23, S25, L72, N73, S74, I75, N76, F77, Y79, E81	Protomer 1 gp120 : T499, R500, C501 Protomer 1 gp41 : G531, A532, M535, T536, L619, S620, W623, D624, K625, Protomer 2 gp41 : L660
6.	10E8 HC: D30, N31, W33, G52C, E53, G54, W55	Protomer 2 gp41 : L660, L661, W666, A667, L669, W670, W672
7.	10E8 HC: K97, Y99, F100A, W100B, G100D, P100F, P100G 10E8 LC: R95B	Protomer 2 gp41 : L669, N671, W672, F673, T676, N677, L679, W680, K683

Figure 6. Structure of Env gp151 MPER ND in complex with bnAbs BG18, VRC01 and 10E8 resolved by cryo-EM. a) Low pass filtered maps of different Fab occupancy states and the location of the bilayer. BG18 Fab is highlighted in green, VRC01 in pink and 10E8 in blue. b) 90° clockwise rotated side views showing the Env tilt angle in relation to lipid bilayer surface. c) Top view and side views of highest resolution maps of both 10E8 occupancy states. Densities are highlighted as

406 follows: gp120 in blue, gp41 in orange, BG18 in green, VRC01 in pink, HC of 10E8 in white, LC
407 of 10E8 in dark grey and MPER peptide in red. d) Highest resolution reconstruction with single
408 10E8 was used for model building. Insets show interfaces of the three bound bnAbs and key amino
409 acid and glycan interactions with BG18 HC (dark green) and LC (light green) in insets 1-2, VRC01
410 HC (magenta) and LC (pink) in insets 3-4, and 10E8 HC (white) and LC (dark grey) in insets 5-7.
411 Glycans are highlighted in purple. Insets 2 and 4 exemplify the electron density used to built
412 interacting glycans (transparent blue. e) Epitope-paratope analysis of 10E8 binding interface
413 shown in d. Contacting residues are separated into three components corresponding insets 5-7. f)
414 Binding pocket of 3BC315 (salmon) CDRH3 with key interactions highlighted. g) gp41 protomer
415 distance analysis in the nanodisc complex structure with 10E8 Fab, and soluble Env structure with
416 3BC315 showing widened interface between protomers A and B due to antibody binding.
417

418

419 **Discussion**

420 Here we present a rigorously optimized glycoprotein nanodisc platform for vaccine design. We
421 show that the assembled GP nanodiscs enable characterization of transmembrane glycoprotein
422 vaccine candidates with key methods in rational, iterative vaccine development that have
423 traditionally been available only to soluble mimics. Applicability of the platform is demonstrated
424 by using SPR to measure antibody kinetics, FACS to characterize new vaccine designs and in vivo
425 antibody responses from preclinical experiments, and cryo-EM to provide structural guidance for
426 immunogen design.

427 In addition to confirming the assembly of EBOV GP in nanodiscs with two Ebola-specific
428 antibodies, we characterized the kinetic landscape of several HIV antibodies binding to HIV Env
429 in nanodiscs. These confirmed that glycan shield modifications and transmembrane domain point
430 mutation identified through directed evolution increased MPER-targeting bnAb 10E8 affinity to
431 prototypical HIV Env MPER-targeting immunogen Env gp151 MPER ND as compared to its
432 design predecessor. While the in vivo responses to the engineered immunogen in humanized
433 mouse model appeared to be outside the targeted C-terminal region of MPER, the identified
434 antibodies will provide guidance for further immunogen engineering. Potential targets of the
435 extracted antibodies include the engineered glycan hole or off-target epitopes at the trimer base.
436 Base of the trimer is partly occluded by the membrane, but some off-target epitopes may still be
437 accessible. This was also indicated by EM-based polyclonal epitope mapping (EMPEM) showing
438 that transmembrane gp151 Env administered as mRNA still elicits base-binding antibodies[15,48].
439 Importantly, using the biotinylated GP nanodisc as FACS probe, we were able to extract antibodies
440 targeting sites that are not fully present in the soluble form of the immunogen. While NHP

441 immunization was beyond the study's scope, we also confirmed GP nanodiscs can be used to
442 identify antigen-specific responses from NHPs, facilitating future studies. Two promising
443 approaches for overcoming the challenges in eliciting MPER targeting antibodies have been
444 recently described, namely priming with germline-targeting immunogen 10E8-GT12[24, 55] or
445 immunizing with MPER peptide alone in liposome formulation[25]. Both solutions present a more
446 accessible MPER peptide for antibody CDRH3. These immunogens can be followed by a next
447 generation Env boost immunogen designs presenting the complete epitope to guide the maturing
448 antibody toward breadth and higher neutralization potency. The analysis and nanodisc GP FACS
449 methods presented here provide vital guidance for these designs.

450 The platform enabled us to determine the structure of Env gp151 MPER ND to 3.5 Å,
451 leading to discovery of structural features that will inform the next generation of immunogens. The
452 structure confirms three HIV bnAb binding sites targeted in ongoing vaccine development projects
453 can be engaged by the same immunogen[56,24, 44]. This further demonstrated that the nanodisc
454 platform has the potential to be used in cryoEMPEM to resolve structures of membrane proximal
455 antibody epitopes from a mixture of specificities from post-immunization serum[57]. As multiple
456 epitopes are now being engineered into Env trimers for germline targeting, it is critical to
457 understand if and how they may compete or synergize. Additional value in using GP nanodiscs is
458 that, in contrast to previous structural studies using soluble mimetics of Env[40, 58], this nanodisc-
459 based structure resembles more closely the native transmembrane protein immunogen[48], which
460 may be important i.e. when assessing glycan engagement in the epitope. Glycan analysis of Env
461 Env gp151 ND and Env gp151 MPER ND agreed with earlier studies showing that when Env is
462 expressed as transmembrane protein, glycan processing resembles more closely that of the virus
463 particle with higher proportion of complex type glycans as in soluble forms[26, 27]. The most
464 significant value of the Env gp151 MPER ND complex cryo-EM structure however is in
465 characterizing the MPER epitope in unprecedented detail. We were able to resolve contacts of
466 10E8 bnAb with the Env ectodomain that have thus far remained elusive in structural studies. A
467 binding pocket for 10E8 FRH3 in the gp120-gp41 interface of the ectodomain, and CDRH1, 2 and
468 3 contacts to the entire MPER domain ending at the lipid bilayer interface, form a continuous
469 network of side chain interactions together spanning 29 AA in the paratope and 26 AA in the
470 epitope. These details can now be used as a structural template to design immunogens for improved
471 engagement of MPER antibodies. Finally, 3D variability analysis of the cryo-EM data illustrates

472 significant remodeling of the N-terminal MPER helix induced by CDRH1 and CDRH2 of 10E8.
473 While care should be taken when interpreting flexible regions, this captures detailed snapshots of
474 the native flexibility of the glycoprotein and MPER domain. The data depicts the range of
475 flexibility and may offer clues how to accommodate native glycoprotein flexibility in vaccine
476 design.

477 In conclusion, the GP nanodisc platform offers a scalable and reproducible solution that
478 provides a more complete and native-like environment for transmembrane glycoprotein vaccine
479 designs. This platform can therefore accelerate the development of next-generation vaccines and
480 may be applicable beyond vaccine development. The described methods present significant
481 additions to the rapidly increasing nanodisc applications in drug discovery technologies[59]. They
482 may be used in workflows for small molecule screening, antibody discovery, and functional studies
483 involving interactions with both extracellular and intracellular binders of any transmembrane
484 protein.

485

486

487 **Methods**

488 This method description aims to provide a complete platform that enables routine use of nanodisc
489 approach for iterative vaccine design using viral glycoproteins. While retaining the versatility of a
490 modular approach, each step is simplified and validated for maximizing reproducibility and
491 scalability.

492

493 **Protein expression and nanodisc assembly**

494 All glycoprotein and antibody constructs were codon optimized for expression in human cells and
495 synthesized and cloned into expression vectors pHLSec (glycoproteins) or its variants pCW-CHIg-
496 hG1, pFabCW pCW-CLig-hL2 or pCW-CLig-hk (IgG heavy chains, Fab heavy chains, lambda
497 light chains and kappa light chains, respectively) by GenScript Biotech. Antibodies were expressed
498 and purified from HEK293F or ExpiCHO cells according to manufacturer's instruction using
499 rProtein A Sepharose Fast Flow resin (Cytiva) as described earlier[24, 44].

500 Soluble Env GP were purified as described earlier[40]. Transmembrane glycoprotein
501 purification method was modified from the earlier protocol[29]. For one liter of transfected cells, 1
502 mg of DNA was mixed with 25 ml of OPTI-MEM medium and sterile filtrated through 0.22 µm

503 filter unit. 3 mg of PEI MAX (Polysciences, #24765) was separately mixed with 25 ml of OPTI-
504 MEM, filtrated and then combined with the DNA. Combined DNA and PEI MAX were then added
505 to HEK293F cells at 1 million/ml density and cells were incubated at 37 °C, 8% CO_2, and 80%
506 humidity under shaking at 180 rpm for 3 days. Cells were harvested by centrifugation at 1500 rcf
507 in 4 °C for 15 min, washed with ~300 ml cold PBS, and centrifuged again at 1500 rcf in 4 °C for
508 15 min. Pelleted cells were lysed with ~5 ml of lysis buffer per gram of cells (50 mM Tris-HCl
509 (pH 7.4), 300 mM NaCl, 0.5% TX-100). Prior to use, approximately 1 protease inhibitor cocktail
510 tablet per 50 ml of lysis buffer, and 2 ml of BioLock (IBA Lifesciences, # 2-0205-050) per liter of
511 cells was added to lysis buffer. Cells were lysed for 1 h at 4 °C in an overhead rotating mixer.
512 Lysed cells were centrifuged for 1 h at 25,000 rcf, followed by filtration of the supernatant through
513 0.22 µm bottle top filtration unit. This resulted in cleared lysate that was passed through Strep-
514 tactin XT 4Flow matrix (IBA Lifesciences, #2-5010-025) in a gravity flow column. Approx. 400
515 µL of drained matrix was used per liter of cells. Matrix was then washed three times with 2 ml of
516 wash buffer 1 (50 mM Tris-HCl (pH 7.4), 300 mM NaCl, 0.1% (w/v) CHAPS, 0.03 mg/mL
517 deoxycholate), three times with 2 ml of wash buffer 2 (50 mM Tris/HCl pH 7.4, 500 mM NaCl, 1
518 mM EDTA, 0.1% DDM, 0.01% CHS, 0.03 mg/ml deoxycholate) and three times 2 ml of wash
519 buffer 3 (50 mM Tris/HCl, pH 7.4, 150 mM NaCl, 0.02% DDM, 0.002% CHS, 0.03 mg/ml
520 deoxycholate). After this, matrix with detergent solubilized GP was transferred to a 5 ml test tube
521 for nanodisc assembly step.

522 Lipid stocks were prepared prior to disc assembly in 1 mM final concentrations. Premade
523 10% DDM/ 0.1% CHS stock (Anatrace, #D310-CH210) was used throughout the study. All lipids
524 in this study were prepared from chloroform stocks (Avanti Polar Lipids). Chloroform was first
525 evaporated under gentle nitrogen stream until transparent film was formed around the glass vial.
526 Lipid film was then rehydrated for 1 h in room temperature in lipid rehydration buffer (50 mM
527 Tris/HCl, pH 7.4, 150 mM NaCl, 0.1% DDM, 0.01% CHS) in a volume bringing the lipid stock
528 concentration to 5 mM. After thorough mixing by vortexing, this stock was diluted further to final
529 lipid stock solution at 1 mM concentration and sonicated with microtip (20-25% intensity, 50%
530 time cycles in 4 °C) until clear. Most lipid stock solutions cleared within 10 – 20 min but with
531 some lipids DDM/CHS amount was increased up to 1%/0.01%. 1 mM lipid stocks were aliquoted
532 and stored up to 6 months at -20°C. A lipid mix roughly following HIV particle lipid composition
533 was used throughout the study and contained 45% DOPC, 7% DOPS, 7% DOPA, 7% DOPE, 7%

534 DOPG, 5% sphingomyelin, 2% PI(4,5)P2, and 20% CHS. Scaffold protein was either produced
535 in-house using standard *E. coli* expression method or purchased from Sigma-Aldrich (membrane
536 scaffold protein 1D1 #M6574 or biotinylated membrane scaffold protein 1D1 BTN #MSP13).
537 Nanodisc batch assembly was done as follows. Strep-tactin matrix with GP bound was
538 drained by gravity flow, after which gravity flow column was capped and 400 µl of wash buffer 3
539 was added to the matrix. 50% matrix slurry was then transferred to a 5 ml test tube. Lipids were
540 added at approx. 350X molar excess and scaffold at 6X molar excess in relation to the glycoprotein.
541 Glycoprotein amount bound to the matrix was estimated with a separate initial experiment where
542 protein was eluted after the last wash step. Minor variations were made to glycoprotein:scaffold
543 and glycoprotein:lipid ratios without significant difference in the final yield. Matrix with
544 glycoprotein, lipids and scaffold was incubated for 1 h at 4°C prior to addition of SM-2 bio-beads
545 (Bio-Rad, #1523920). Bio-beads were activated according to the manufacturer's instructions in
546 methanol followed by extensive wash with deionized water. Bio-beads were added to approx. 50%
547 v/v with the nanodisc assembly mixture. i.e. if the total volume of the assembly reaction was 1.5
548 ml, final volume after bio-bead addition in the 5 ml test tube was ~3 ml. Detergent was then
549 removed by incubation in a rotating shaker overnight at 4°C. The following day an additional
550 ~20% of the total reaction volume of fresh bio-beads were added, followed by an additional 1 h
551 incubation at room temperature to ensure complete removal of detergent. Next, contents of the test
552 tube were transferred to a new gravity flow column with a pipette tip with the first ~2 mm cut off
553 to allow pipetting biobeads and matrix. Mixture was washed in column twice with 4 ml of TBS
554 and eluted with Strep-tactin elution buffer BXT in 500 µl fractions. A280 of eluted fractions were
555 monitored and fractions containing protein were pooled and concentrated to <500 µl for SEC
556 performed using a Superose 6 Increase 10/300 column (Cytiva) at 0.75ml/min in TBS. SDS-PAGE
557 and ns EM analysis were used to confirm presence of glycoprotein and scaffold protein, typical
558 disc appearance in ns EM 2D class averages and glycoprotein on disc.
559 For structural biology purposes, Fabs were added to the GP nanodiscs after the assembly
560 while nanodisc was still bound to strep-tactin matrix. After the second addition of bio-beads, each
561 Fab was added at ~10X molar excess and the mixture was incubated for an additional 2h at room
562 temperature. Complex elution and following steps were identical as described above for
563 unliganded glycoprotein nanodiscs. Fractions were pooled after SEC and sample was concentrated

564 either to 1 mg/ml for FACS, SPR and other purposes, or up to 11 mg/ml for cryo-EM sample
565 preparation.

566 **Identification of R696S mutation on HIV Env by mammalian directed evolution.**
567 A 250 amino acid long site-saturation mutagenesis (NNK) scan of gp41 was synthesized at SGI-
568 DNA. A fragment of the library containing NNKs from positions T606 to F699 (94 positions) was
569 cloned into BG505 MD39.2 gp151. This library was stably integrated into 293T-rtTA3G cell line
570 using the lentivirus-based mammalian display protocol described previously[34, 40,35]. After inducing
571 library expression overnight, the cells were stained with 10E8 IgG and PGT145 Fab and those
572 with highest binding to 10E8 that were also positive for PGT145 were sorted. After three rounds
573 of sorting, the library DNA was extracted and sequenced by Sanger sequencing. 8 of 19 sequences
574 had a mutation at position 696, which was mutated from R to S, A, V, I and L. The most frequent
575 mutation, R696S, was selected for further characterization.
576

577 **Mass spectrometry**
578 **Proteinase K treatment and deglycosylation.** HIV Env glycoprotein (when membrane bound,
579 denatured in 6 M urea) was exchanged to water using Microcon Ultracel PL-10 centrifugal filter.
580 Glycoprotein was reduced with 5 mM tris(2-carboxyethyl)phosphine hydrochloride (TCEP-HCl)
581 and alkylated with 10 mM 2-Chloroacetamide in 100 mM ammonium acetate for 20 min at room
582 temperature (RT, 24 °C). Initial protein-level deglycosylation was performed using 250 U of Endo
583 H for 5 µg trimer, for 1 h at 37 °C. Glycoprotein was digested with 1:25 Proteinase K (PK) for 30
584 min at 37 °C. PK was denatured by incubating at 90 °C for 15 min, then cooled to RT. Peptides
585 were deglycosylated again with 250 U Endo H for 1 h at 37 °C, then frozen at –80 °C and
586 lyophilized. 100 U PNGase F was lyophilized, resuspended in 20 µl 100 mM ammonium
587 bicarbonate prepared in $H_2{}^{18}O$, and added to the lyophilized peptides. Reactions were then
588 incubated for 1 h at 37 °C, subsequently analyzed by LC-MS/MS.
589

590 **LC-MS/MS.** Samples were analyzed on an Q Exactive HF-X mass spectrometer. Samples were
591 injected directly onto a 25 cm, 100 µm ID column packed with BEH 1.7 µm C18 resin. Samples
592 were separated at a flow rate of 300 nL/min on an EASY-nLC 1200 UHPLC. Buffers A and B
593 were 0.1% formic acid in 5% and 80% acetonitrile, respectively. The following gradient was used:
594 1–25% B over 160 min, an increase to 40% B over 40 min, an increase to 90% B over another 10

min and 30 min at 90% B for a total run time of 240 min. Column was re-equilibrated with solution A prior to the injection of sample. Peptides were eluted from the tip of the column and nanosprayed directly into the mass spectrometer by application of 2.8 kV at the back of the column. The mass spectrometer was operated in a data dependent mode. Full MS1 scans were collected in the Orbitrap at 120,000 resolution. The ten most abundant ions per scan were selected for HCD MS/MS at 25 NCE. Dynamic exclusion was enabled with exclusion duration of 10 s and singly charged ions were excluded.

Data Processing. Protein and peptide identification were done with Integrated Proteomics Pipeline (IP2). Tandem mass spectra were extracted from raw files using RawConverter [60] and searched with ProLuCID[61] against a database comprising UniProt reviewed (Swiss-Prot) proteome for Homo sapiens (UP000005640), UniProt amino acid sequences for Endo H (P04067), PNGase F (Q9XBM8), and Proteinase K (P06873), amino acid sequences for the examined proteins, and a list of general protein contaminants. The search space included no cleavage-specificity. Carbamidomethylation (+57.02146 C) was considered a static modification. Deamidation in presence of $H_2{}^{18}O$ (+2.988261 N), GlcNAc (+203.079373 N), oxidation (+15.994915 M) and N-terminal pyroglutamate formation (–17.026549 Q) were considered differential modifications. Data was searched with 50 ppm precursor ion tolerance and 50 ppm fragment ion tolerance. Identified proteins were filtered using DTASelect2[62] and utilizing a target-decoy database search strategy to limit the false discovery rate to 1%, at the spectrum level[63]. A minimum of 1 peptide per protein and no tryptic end per peptide were required and precursor delta mass cut-off was fixed at 15 ppm. Statistical models for peptide mass modification (modstat) were applied. Census2[64] label-free analysis was performed based on the precursor peak area, with a 15 ppm precursor mass tolerance and 0.1 min retention time tolerance. “Match between runs” was used to find missing peptides between runs. Data analysis using GlycoMSQuant [42] was implemented to automate the analysis. GlycoMSQuant summed precursor peak areas across replicates, discarded peptides without NGS, discarded misidentified peptides when N-glycan remnant-mass modifications were localized to non-NGS asparagines and corrected/fixed N-glycan mislocalization where appropriate.

625 **SPR**

626 The kinetics and binding affinities of antibody-antigen interactions were analyzed using either
627 ProteOn XPR36 system (Bio-Rad) or Carterra LSA. TBS pH 7.4 (20 mM Tris, 150 mM NaCl)
628 supplemented with BSA at 1 mg/ml without detergents was used as running buffer in all
629 experiments. In ProteOn XPR36, HC30M XanTec sensor chips were utilized. In modalities B and
630 C, anti-human IgG (Fc) antibody (GE, #BR-1008-39) was used for capturing IgG (ligand) at low
631 densities with nanodisc GP as the analyte. In modality A, anti-Strep-tag antibody (pAb, rabbit,
632 GenScript, #A00875) was used for capturing Strep-tagged nanodiscs GP (ligand) followed by GP
633 specific Fab as the analyte. Approximately 6000-8000 response units (RU) of the capture antibody
634 were covalently attached to the sensor surface using EDC-NHS chemistry. For IgG-antigen
635 interaction studies, approximately 50 to 100 RUs of IgGs at a concentration of 0.3 µg/ml were
636 immobilized on each flow cell. For Fab-antigen interaction studies, approximately 300 to 400 RUs
637 of antigen at 10 µg/ml were captured on each flow cell. Analytes were introduced to the flow cell
638 at a rate of 30 µl/min for 3 minutes, followed by a dissociation phase of 5 minutes. Regeneration
639 was performed with 1.7% or 0.85% phosphoric acid, each with a contact time of 60-180 seconds,
640 repeated four times per cycle. Data analysis was conducted using ProteOn Manager software (Bio-
641 Rad), including raw sensogram processing, interspot referencing, and column double referencing.
642 Equilibrium or kinetic fits were performed using the Langmuir model as needed.

643

644 Kinetics and affinity of antibody-antigen interactions on Carterra LSA using CMDP Sensor Chip
645 (Carterra) for capture IgG – flow nanodisc (modality B) was done as follows. Chip surfaces were
646 prepared according to Carterra software instructions. In a typical experiment approx. 500-700 RU
647 of capture antibody (SouthernBiothech, # 2047-01) in 10 mM Sodium Acetate pH 4.5 was amine
648 coupled on CMDP chip placing special care on concentration range of the amine coupling reagents.
649 We used N-Hydroxysuccinimide (NHS) and 1-Ethyl-3-(3-dimethylaminopropyl)
650 carbodiimidehydrochloride (EDC) from Amine Coupling Kit (GE, #BR-1000-50). Highest
651 coupling levels of capture antibody were achieved by using 10 times diluted NHS and EDC during
652 surface preparation runs as compared to kit instruction (10 ml of water each to give 11.5 mg/ml
653 and 75 mg/ml respectively according to kit instructions). Thus, the concentrations of NHS and
654 EDC were 1.15 mg/ml and 7.5 mg/ml and the activation time was reduced to 1 min. The
655 concentrated stocks of NHS and EDC were stored frozen in -20 °C for up to 2 months without

656 noticeable loss of activity. The capture antibody was used at concentration 25 µg/ml with 10
657 minutes contact time. Phosphoric Acid 1.7% was used as a regeneration solution with 60 seconds
658 contact time and injected three times per cycle. Concentration of ligands were approximately 1
659 µg/ml and contact time was 5 min. Raw sensograms were analyzed using Kinetics software
660 (Carterra) with interspot and blank double referencing, and Langmuir model. Analyte
661 concentrations were quantified on NanoDrop 2000c spectrophotometer using absorption signal at
662 280 nm. Analytes were buffer exchanged into the running buffer using dialysis. In a typical run,
663 we covered a broad range of affinities and used two referencing practices depending on the off-
664 rate of the ligand. For fast off-rate (faster than 9 x 10^{-3} 1/s), we use automated batch referencing
665 that includes overlay y-aline and higher analyte concentrations. For slow off-rates (9 x 10^{-3} 1/s or
666 less), we use manual process referencing that includes serial y-align and lower analyte
667 concentrations. After automated data analysis by Kinetics software, we performed additional
668 filtering to remove datasets with highest response signals smaller than signals from negative
669 controls using R-script.
670
671 **FACS**
672 **Validation of Env-Nanodisc proteins as fluorescent baits**
673 Streptavidin (SA) conjugated-antigen baits were prepared by combining biotinylated Env-
674 nanodisc or empty nanodisc with fluorescent SA at room temperature for at least 1 hr in dark at a
675 bait:SA molar ratio of 2:1. Control breads for FACS were generated by conjugating various bnAbs
676 to compensation beads. Mouse anti-human IgG (BD Biosciences, # 555784) was first captured on
677 to anti-mouse IgK compensation beads (BD Biosciences, # 552843), followed by a wash step and
678 a secondary capture of bnAbs of interest. VRC01-expressing Ramos cells [43], C57BL/6 splenocytes,
679 and the prepared bnAb-conjugated beads were incubated with the nanodisc GP:SA baits at a bait
680 concentration of 10-50 nM in the final staining volume for 30 min at 4 °C in the dark. Data were
681 acquired on a BD FACS Melody, and analzyed in FlowJo v10 (FlowJo, LLC).
682
683 **Mouse immunization studies**
684 hD3-3/JH6 mice were immunized as previously described[24]. Briefly, homozygous hD3-3/JH6
685 mice were injected with 10 µg (50 µl total volume) of Moderna mRNA LNPs encoding Env gp151
686 MPER I.M. under anesthesia (5% isoflurane induction) in the left quadriceps muscle. After six

687 weeks, mice were euthanized with compressed CO_2 (100%) in a clear chamber to allow for
688 visualization of respiration and subsequent death via respiratory cessation. Blood was collected
689 from the chest cavity prior to the removal of the spleen and lymph nodes (mesenteric, inguinal,
690 and popliteal). Tissues were placed in 3 mL FACS buffer (1 X PBS Ca/Mg^{++} free, 1 mM EDTA,
691 25 mM HEPES, pH 7.0, 1% heat-inactivated FBS) on ice and tissues were disassociated using the
692 rough ends of two sandblasted microscope slides, followed by centrifugation (460 rcf for 5 minutes
693 at 4 °C). Red blood cell lysis was performed using 1 mL of ACK buffer (Quality Biological) for 2
694 minutes on ice before lysis was halted by adding 14 mL FACS buffer per sample. Post lysis and
695 centrifugation (460 xg for 5 minutes), cells were resuspended in 3 mL Bambanker freezing
696 medium (Bulldog Bio) prior to filtration through a cotton-plugged, borosilicate pasteur pipette into
697 a borosilicate glass test tube. 1 mL filtered-cell solution was subsequently divided into three
698 cryovials/mouse, which were precooled in a styrofoam rack on dry ice. Cells were stored at -80 °C
699 for 2-7 days prior to long-term storage in liquid nitrogen. All work followed IACUC guidelines
700 associated with animal protocol number 20-0001.
701
702 **Mouse sample preparation and B cell sorting**
703 Mouse frozen mouse splenoctyes and lymphocytes were thawed and stained as previously
704 described[24, 56]. Briefly, after thawing and counting, total B cells were isolated by negative selection
705 using the EasySep Mouse Pan-B Cell Isolation Kit (StemCell, #19844) according to
706 manufacturer's instructions. SA-conjugated baits were prepared as described above. Wildtype
707 antigen baits were conjugated to BV421-SA (BioLegend, #405225) and AlexaFluor 647SA
708 (Invitrogen, #S21374), while epitope knockout (KO) baits were conjugated to hashtagged
709 TotalSeq-C PE SA (BioLegend, #405261). Purified B cells were stained at 4 °C in dark, with
710 appropriate baits and antibody master-mix consisting of FITC anti-CD19 (BioLegend, #152404),
711 BV786 anti-IgM (BD Biosciences, #743328), PerCP-Cy5.5 anti-IgD (BD Biosciences, #564273),
712 APC-Cy7 anti-F4/80 (BioLegend, #123118), APC-Cy7 anti-CD11c (BD Biosciences, #561241),
713 APC-Cy7 anti-Ly6C (BD Biosciences, #557661), APC-H7 anti-CD8a (BD Biosciences,
714 #560182), and APC-H7 anti-CD4 (BD Biosciences, #560181), all used at 1:100 dilution and
715 prepared in FACS buffer (1% v/v heat inactivated FBS, 1 mM EDTA, 1 mM HEPES in 1x DPBS).
716 The KO bait was first added to cells with the antibody master mix for 15 minutes, followed by the
717 addition of WT baits for an additional 30 min. Each bait was used at final bait concentration of

718 100 nM in the staining volume or 0.5 µg per sample. During the addition of antibody master mix,
719 a unique TotalSeq-C anti-mouse hashtag antibody (BioLegend) was added to each sample at a
720 concentration of 2.5 µL / up to 20 million cells. Following antibody staining, 1 mL of 1:300
721 live/dead stain diluted in FACS buffer (Invitrogen, #L34966) was added to each sample for an
722 additional 15 minutes at 4 °C, then washed with 10 mL of FACS buffer. Cells were resuspended
723 in a final volume of 500 µL FACS buffer and sorted on a BD FACS Melody. Cells were bulk
724 sorted into a 4 °C chilled PCR plate well containing 20 µL of 0.2 µm filtered FBS, and processed
725 for BCR sequencing via the 10x Genomics Single Cell Immune Profiling according to kit
726 protocols, with minor modifications outlined previously[65]. Pooled libraries were sequenced on an
727 Illumina NextSeq 2000 using a 100-cycle P3 reagent kit (Illumina, #20040559).
728

729 **BCR sequence analysis**

730 Sequence analysis Raw sequencing data were demultiplexed, processed into assembled VDJ
731 contigs and counts matrix files, and assigned to specific animal IDs based on TotalSeq-C antibody
732 hashtag counts using Cell Ranger (v6.1) and scab as previously described[65]. Gene assignment,
733 annotation, and formatting into Adaptive Immune Receptor Repertoire (AIRR) format[66] for paired
734 heavy and light chain antibody sequences was performed using Sequencing Analysis and Data
735 library for Immunoinformatics Exploration (SADIE) with a previously described custom germline
736 reference database that included all known mouse antibody genes plus the human IGHD3-3 and
737 IGHJ6 genes that were knocked into hD3-3/JH6 mice[24]. Eight antibodies from each animal were
738 randomly selected for in vitro analysis, except for one animal from which only two total
739 heavy/light pairs were recovered. In addition, 12 antibodies with long HCDR3s (>19 aa) were
740 selected for in vitro characterization.
741

742 **NHP Flow Cytometry**

743 Frozen NHP PBMC samples were thawed in RPMI media with 10% FBS, 1% GlutaMAX,
744 and 1% Penicillin/Streptomycin (R10). NHP samples used in this study were from animals that
745 were reported in previous studies [47,48]. The recovered cells were then stained with the appropriate
746 antibody panel. Fluorescent antigen probes were constructed by combining fluorophore-
747 conjugated streptavidin and biotinylated nanodisc GP or soluble Env probes with an appropriate
748 volume of PBS in small increments across 45 minutes at room temperature (RT). Thawed cells

749 were incubated with probes for thirty minutes at 4°C. A master mix of surface staining antibodies
750 was then added and incubated for thirty minutes at 4°C. Cells were washed and prepared for
751 acquisition on Cytek Aurora (Cytek Biosciences). The following reagents were used in the
752 PBMC staining panel: Alexa Fluor 647 Streptavidin (BioLegend #405237), BV421 Streptavidin
753 (BioLegend #405225), PE Streptavidin (BioLegend #405245), PE-Cy7 Streptavidin (BioLegend
754 #405206), BV711 Streptavidin (BioLegend #405241), BUV615 Streptavidin (BioLegend
755 #613013), Viability eFluor780 (1:2000, Invitrogen #65-0865-14), CD3 BV510 (1:100, BD
756 Biosciences #569488), CD14 BV510 (1:100, BioLegend #301842), CD8a BV510 (1:100, BD
757 Biosciences #563256), CD16 BV510 (1:100, BioLegend #302048), CD20 (1:100, BUV395 BD
758 Biosciences #563782), IgG BV605 (1:100, BD Biosciences #563246), and IgD AF488 (1:50,
759 Southern Biotech #2030-30).
760
761 **EM**
762 Negative stain EM was used for quality control of nanodisc assembly and for initial assessment of
763 antibody complexes for cryo-EM. Glycoprotein nanodisc or nanodisc with three fold molar excess
764 of Fab was applied to 400 mesh size Cu grid at 0.04-0.06 mg/ml concentration, blotted off with
765 filter paper and stained with 2% uranyl formate for 60 s. NsEM data was collected on a Tecnai
766 Spirit microscope operating at 120 keV, using a Tietz 4k × 4k TemCam-F416 CMOS camera and
767 Leginon automated image collection software[66]. Data was processed using Relion 3.0 image
768 processing pipeline[67].
769 For cryo-EM, nanodisc was complexed with 10X molar excess of VRC01, BG18 and 10E8 Fabs
770 after batch nanodisc assembly, while bound to affinity matrix. Eluted complex was then SEC
771 purified (Superose 6 Increase column. Cytiva), concentrated to 8 mg/ml and frozen on graphene
772 oxide grids (GO on Quantifoils R1.2/1.3, Cu, 400 mesh, Electron Microscopy Sciences) with 30
773 sec wait time, blot force of 0, and blot time of 2.5-3 s. Fluorinated Fos-Choline-8 (Anatrace #
774 F300F) was added to sample immediately prior to freezing to a final concentration of 3 mM. GO
775 grids, high sample concentration and fluorinated Fos-Choline-8 were necessary to prevent freeze-
776 denaturation, ensure high particle count per micrograph and prevent orientation bias. 11,871
777 micrographs were collected at pixel size 0.718 Å using a Thermo Fisher Scientific Glacios 2
778 microscope operating at 200 kV and equipped with a Thermo Fisher Scientific Falcon 4i camera
779 using a total dose of 44.89 e-/Å2. Automated data collection was performed using the EPU

780 software (Thermo Fisher Scientific) and images were written in the EER frame format.
781 Micrographs were preprocessed using cryoSPARC Live[67], including motion and CTF correction.
782 Briefly, particles were picked with Topaz[68] after training the neural network with a subset of
783 particles first picked with blob picker. Picked particles were subjected to 3 rounds of 2D
784 classification to obtain a final particle stack of 317,792 particles. These were then extracted from
785 micrographs using a box size of 540 pix. Maps containing one or two copies of 10E8 Fab were
786 separated using heterogenous reconstruction and 3D classification tasks. A class with 7,964
787 particles containing two copies of 10E8 was refined to 4.3Å resolution. A class with 111,002
788 particles containing single 10E8 was examined with 3D variability analysis[69]. Further
789 classification resulted in final, cleaned particle stack containing 63,366 particles which was then
790 subjected to Non-Uniform Refinement[70] and used for atomic model building. Data collection and
791 processing stats are summarized in Supplementary Table 1. Atomic model building was initiated
792 by docking in available structures of 10E8 Fab (PDB 4G6F), BG18 Fab (PDB 6DFG), VRC01
793 Fab (PDB 3NGB) and an AlphaFold3[71] -generated model of the trimer into the map using
794 ChimeraX[72]. Manual adjustment was done using Coot[73] and further refinement was done using
795 Phenix Real Space Refine[74] and Rosetta Relax[75]. Final model statistics are summarized in
796 Supplementary Table 1.
797 The soluble gp140 (MD39.3) cryo-EM structure was done as follows: VRC01, BG18 and
798 3BC315 Fabs were added at 4.3X molar excess to purified Env glycoprotein. The complex was
799 purified using a HiLoad Superdex 200 16/600 pg column (Cytiva) and concentrated to 10 mg/ml.
800 Samples were vitrified using a Thermo Fisher Scientific Vitrobot Mark IV operating at 100%
801 humidity, 4°C and 3-6 s blot times, on UltrAuFoil 1.2/1.3-300 holey gold film grids (Electron
802 Microscopy Sciences). Prior to grid application, lauryl maltose neopentyl glycol (LMNG) was
803 added to a final concentration of 0.005 mM. Imaging was performed using the same microscope
804 and conditions as for Env gp151 MPER ND complex. After initial cryoSPARC particle picking
805 using Blob Picker, templates were selected from 2D classification and used for Template Picker.
806 A total of 886,907 particles were extracted using a box size of 576 downsampled to 144. After
807 additional rounds of 2D classification, an Ab Initio Reconstruction was performed, followed by
808 Non-Uniform refinement. A single 3BC315 Fab was visible in the C1 reconstruction. A mask was
809 created over 3BC315 and focused 3D classification performed to remove trimers with no 3BC315
810 particles. A final stack of 243,503 were re-extracted and downsampled to box size 400 (resulting

811 in pixel size of 1.034 Å) and subjected to Non-Uniform Refinement which resulted in a 3.1 Å
812 reconstruction. Model building was performed as above and final model statistics are summarized
813 in Supplementary Table 1.
814 Maps and models have been deposited to the EMDB and PDB, respectively, under the
815 accession codes listed in Supplementary Table 1.
816
817 **Acknowledgements**
818 We thank Nicole Doria-Rose for providing the VRC01 expressing Ramos cell line. We thank Brian
819 Briney for providing access to Illumina NextSeq 2000 sequencer. We thank Daniel Murin for
820 providing Ebola GP specific antibodies.
821
822 **Funding**
823 This work was supported by National Institute of Allergy and Infectious Diseases UM1 AI144462
824 (Scripps Consortium for HIV/AIDS Vaccine Development; to J.C.P., T.S., A.B.W., and W.R.S),
825 R01 AI147826 (to W.R.S.); Bill and Melinda Gates Foundation Collaboration for AIDS Vaccine
826 Discovery awards (INV-007522 and INV-008813 for the IAVI NAC Center to A.B.W. and
827 W.R.S.; and INV-002916 to A.B.W.); the IAVI Neutralizing Antibody Center (to A.B.W. and
828 W.R.S.); and the Alexander von Humboldt Foundation (T.S.).
829
830 **Competing interests**: J.M.S and W.R.S. are inventors on a patent for the BG505 MD39 and N332-
831 GT5 immunogens (US11203617B2 and US20230190914A1). S.H. and W.R.S. are employees and
832 shareholders of Moderna, Inc. All other authors declare no competing interests.
833
834 **Author contributions:** K.R. designed nanodisc assembly workflow, performed cryo-EM
835 imaging, data processing and structural analysis, and wrote the manuscript. A.L. and O.K.
836 established conditions and conducted SPR assays. G.O. Supervised cryo-EM imaging and data
837 processing and built 3D models. C.F. performed and J.H.L. and D.S. supervised establishing
838 conditions for mouse B cell FACS experiments. J.M.S., O.S. and T.S. contributed to immunogen
839 design. S.B. and J.K.D. performed, and J.R.Y. and J.C.P. supervised mass spectrometry glycan
840 profiling. P.J.M. and M.S. performed, and S.C. supervised NHP B cell FACS analysis. S.W. and
841 A.G. contributed, and G.O. and A.B.W. supervised cryo-EM imaging, data processing and model

842 building. D.L. performed nanodisc assembly reactions. P.K. and S.T. performed mouse
843 immunizations. D.L., E.G., R.T., S.E., N.A., D.G. and M.K. produced purified proteins. W-H.L.
844 contributed to cryo-EM sample preparation. S.H. provided mRNA immunogens. T.S., A.B.W. and
845 W.R.S. supervised the study. G.O., T.S., A.B.W. and W.R.S. edited the manuscript. All authors
846 reviewed the manuscript.
847

848 **References**

849 1. Bayburt, T.H., Grinkova, Y.V. & Sligar, S.G. Self-assembly of discoidal phospholipid
850 bilayer nanoparticles with membrane scaffold proteins. *Nano Letters* **2**, 853-856 (2002).
851 2. Dorr, J.M. et al. The styrene-maleic acid copolymer: a versatile tool in membrane
852 research. *Eur Biophys J* **45**, 3-21 (2016).
853 3. Carlson, M.L. et al. The Peptidisc, a simple method for stabilizing membrane proteins in
854 detergent-free solution. *Elife* **7** (2018).
855 4. Frauenfeld, J. et al. A saposin-lipoprotein nanoparticle system for membrane proteins.
856 *Nat Methods* **13**, 345-351 (2016).
857 5. Pettersen, J.M., Yang, Y. & Robinson, A.S. Advances in nanodisc platforms for
858 membrane protein purification. *Trends Biotechnol* **41**, 1041-1054 (2023).
859 6. Sligar, S.G. & Denisov, I.G. Nanodiscs: A toolkit for membrane protein science. *Protein*
860 *Sci* **30**, 297-315 (2021).
861 7. Denisov, I.G. & Sligar, S.G. Nanodiscs for structural and functional studies of membrane
862 proteins. *Nat Struct Mol Biol* **23**, 481-486 (2016).
863 8. Trahey, M. et al. Applications of Lipid Nanodiscs for the Study of Membrane Proteins by
864 Surface Plasmon Resonance. *Curr Protoc Protein Sci* **81**, 29 13 21-29 13 16 (2015).
865 9. Bocquet, N. et al. Real-time monitoring of binding events on a thermostabilized human
866 A2A receptor embedded in a lipid bilayer by surface plasmon resonance. *Biochim*
867 *Biophys Acta* **1848**, 1224-1233 (2015).
868 10. Gluck, J.M., Koenig, B.W. & Willbold, D. Nanodiscs allow the use of integral membrane
869 proteins as analytes in surface plasmon resonance studies. *Anal Biochem* **408**, 46-52
870 (2011).
871 11. Wang, M.Y. et al. SARS-CoV-2: Structure, Biology, and Structure-Based Therapeutics
872 Development. *Front Cell Infect Microbiol* **10**, 587269 (2020).
873 12. Pallesen, J. et al. Immunogenicity and structures of a rationally designed prefusion
874 MERS-CoV spike antigen. *Proc Natl Acad Sci U S A* **114**, E7348-E7357 (2017).
875 13. Kirchdoerfer, R.N. et al. Pre-fusion structure of a human coronavirus spike protein.
876 *Nature* **531**, 118-121 (2016).
877 14. Shepherd, B.O., Chang, D., Vasan, S., Ake, J. & Modjarrad, K. HIV and SARS-CoV-2:
878 Tracing a Path of Vaccine Research and Development. *Curr HIV/AIDS Rep* **19**, 86-93
879 (2022).
880 15. Pardi, N., Hogan, M.J., Porter, F.W. & Weissman, D. mRNA vaccines - a new era in
881 vaccinology. *Nat Rev Drug Discov* **17**, 261-279 (2018).
882 16. Chaudhary, N., Weissman, D. & Whitehead, K.A. mRNA vaccines for infectious
883 diseases: principles, delivery and clinical translation. *Nat Rev Drug Discov* **20**, 817-838
884 (2021).
885 17. Guenaga, J. et al. mRNA lipid nanoparticles expressing cell-surface cleavage
886 independent HIV Env trimers elicit autologous tier-2 neutralizing antibodies. *Front*
887 *Immunol* **15**, 1426232 (2024).
888 18. Benton, D.J. et al. Influenza hemagglutinin membrane anchor. *Proc Natl Acad Sci U S A*
889 **115**, 10112-10117 (2018).
890 19. Lopez, C.A., Alam, S.M., Derdeyn, C.A., Haynes, B.F. & Gnanakaran, S. Influence of
891 membrane on the antigen presentation of the HIV-1 envelope membrane proximal
892 external region (MPER). *Curr Opin Struct Biol* **88**, 102897 (2024).

893 20. Liu, H., Su, X., Si, L., Lu, L. & Jiang, S. The development of HIV vaccines targeting
894 gp41 membrane-proximal external region (MPER): challenges and prospects. *Protein*
895 *Cell* **9**, 596-615 (2018).
896 21. Guthmiller, J.J. et al. Broadly neutralizing antibodies target a haemagglutinin anchor
897 epitope. *Nature* **602**, 314-320 (2022).
898 22. Zhang, L. et al. An MPER antibody neutralizes HIV-1 using germline features shared
899 among donors. *Nat Commun* **10**, 5389 (2019).
900 23. Krebs, S.J. et al. Longitudinal Analysis Reveals Early Development of Three MPER-
901 Directed Neutralizing Antibody Lineages from an HIV-1-Infected Individual. *Immunity*
902 **50**, 677-691 e613 (2019).
903 24. Schiffner, T. et al. Vaccination induces broadly neutralizing antibody precursors to HIV
904 gp41. *Nat Immunol* **25**, 1073-1082 (2024).
905 25. Williams, W.B. et al. Vaccine induction of heterologous HIV-1-neutralizing antibody B
906 cell lineages in humans. *Cell* **187**, 2919-2934 e2920 (2024).
907 26. Cao, L. et al. Differential processing of HIV envelope glycans on the virus and soluble
908 recombinant trimer. *Nat Commun* **9**, 3693 (2018).
909 27. Rantalainen, K. et al. Co-evolution of HIV Envelope and Apex-Targeting Neutralizing
910 Antibody Lineage Provides Benchmarks for Vaccine Design. *Cell Rep* **23**, 3249-3261
911 (2018).
912 28. Torrents de la Pena, A. et al. Similarities and differences between native HIV-1 envelope
913 glycoprotein trimers and stabilized soluble trimer mimetics. *PLoS Pathog* **15**, e1007920
914 (2019).
915 29. Rantalainen, K. et al. HIV-1 Envelope and MPER Antibody Structures in Lipid
916 Assemblies. *Cell Rep* **31**, 107583 (2020).
917 30. Nakatani-Webster, E., Hu, S.L., Atkins, W.M. & Catalano, C.E. Assembly and
918 characterization of gp160-nanodiscs: A new platform for biochemical characterization of
919 HIV envelope spikes. *J Virol Methods* **226**, 15-24 (2015).
920 31. Bhattacharya, P. et al. Nanodisc-incorporated hemagglutinin provides protective
921 immunity against influenza virus infection. *J Virol* **84**, 361-371 (2010).
922 32. Mabrouk, M.T. et al. Circularized Nanodiscs for Multivalent Mosaic Display of SARS-
923 CoV-2 Spike Protein Antigens. *Vaccines (Basel)* **11** (2023).
924 33. Yang, S. et al. Dynamic HIV-1 spike motion creates vulnerability for its membrane-
925 bound tripod to antibody attack. *Nat Commun* **13**, 6393 (2022).
926 34. Steichen, J.M. et al. HIV Vaccine Design to Target Germline Precursors of Glycan-
927 Dependent Broadly Neutralizing Antibodies. *Immunity* **45**, 483-496 (2016).
928 35. Willis, J.R. et al. Human immunoglobulin repertoire analysis guides design of vaccine
929 priming immunogens targeting HIV V2-apex broadly neutralizing antibody precursors.
930 *Immunity* **55**, 2149-2167 e2149 (2022).
931 36. Puthenveetil, R., Nguyen, K. & Vinogradova, O. Nanodiscs and Solution NMR:
932 preparation, application and challenges. *Nanotechnol Rev* **6**, 111-126 (2017).
933 37. Gu, S., Huang, M. & Handel, T.M. On-bead purification and nanodisc reconstitution of
934 human chemokine receptor complexes for structural and biophysical studies. *STAR*
935 *Protoc* **4**, 102460 (2023).
936 38. Dev, J. et al. Structural basis for membrane anchoring of HIV-1 envelope spike. *Science*
937 **353**, 172-175 (2016).

938 39. Rutten, L. et al. Structure-Based Design of Prefusion-Stabilized Filovirus Glycoprotein
939 Trimers. *Cell Rep* **30**, 4540-4550 e4543 (2020).
940 40. Steichen, J.M. et al. A generalized HIV vaccine design strategy for priming of broadly
941 neutralizing antibody responses. *Science* **366** (2019).
942 41. Xie, Z. et al. mRNA-LNP HIV-1 trimer boosters elicit precursors to broad neutralizing
943 antibodies. *Science* **384**, eadk0582 (2024).
944 42. Baboo, S. et al. DeGlyPHER: An Ultrasensitive Method for the Analysis of Viral Spike
945 N-Glycoforms. *Anal Chem* **93**, 13651-13657 (2021).
946 43. Hossain, M.A. et al. B cells expressing IgM B cell receptors of HIV-1 neutralizing
947 antibodies discriminate antigen affinities by sensing binding association rates. *Cell Rep*
948 **39**, 111021 (2022).
949 44. Steichen, J.M. et al. Vaccine priming of rare HIV broadly neutralizing antibody
950 precursors in nonhuman primates. *Science* **384**, eadj8321 (2024).
951 45. Vazquez Bernat, N. et al. Rhesus and cynomolgus macaque immunoglobulin heavy-chain
952 genotyping yields comprehensive databases of germline VDJ alleles. *Immunity* **54**, 355-
953 366 e354 (2021).
954 46. Chernyshev, M., Kaduk, M., Corcoran, M. & Karlsson Hedestam, G.B. VDJ Gene Usage
955 in IgM Repertoires of Rhesus and Cynomolgus Macaques. *Front Immunol* **12**, 815680
956 (2021).
957 47. Phung, I. et al. A combined adjuvant approach primes robust germinal center responses
958 and humoral immunity in non-human primates. *Nat Commun* **14**, 7107 (2023).
959 48. Ramezani-Rad, P. et al. Vaccination with mRNA-encoded membrane-bound HIV
960 Envelope trimer induces neutralizing antibodies in animal models. *bioRxiv* (2025).
961 49. Irimia, A. et al. Lipid interactions and angle of approach to the HIV-1 viral membrane of
962 broadly neutralizing antibody 10E8: Insights for vaccine and therapeutic design. *PLoS*
963 *Pathog* **13**, e1006212 (2017).
964 50. Soto, C. et al. Developmental Pathway of the MPER-Directed HIV-1-Neutralizing
965 Antibody 10E8. *PLoS One* **11**, e0157409 (2016).
966 51. Rujas, E. et al. Structural basis for broad neutralization of HIV-1 through the molecular
967 recognition of 10E8 helical epitope at the membrane interface. *Sci Rep* **6**, 38177 (2016).
968 52. Huang, J. et al. Broad and potent neutralization of HIV-1 by a gp41-specific human
969 antibody. *Nature* **491**, 406-412 (2012).
970 53. Lee, J.H. et al. Antibodies to a conformational epitope on gp41 neutralize HIV-1 by
971 destabilizing the Env spike. *Nat Commun* **6**, 8167 (2015).
972 54. Pancera, M. et al. Structure and immune recognition of trimeric pre-fusion HIV-1 Env.
973 *Nature* **514**, 455-461 (2014).
974 55. Ray, R. et al. Affinity gaps among B cells in germinal centers drive the selection of
975 MPER precursors. *Nature Immunology* **25** (2024).
976 56. Cottrell, C.A. et al. Heterologous prime-boost vaccination drives early maturation of HIV
977 broadly neutralizing antibody precursors in humanized mice. *Sci Transl Med* **16**,
978 eadn0223 (2024).
979 57. Antanasijevic, A. et al. Polyclonal antibody responses to HIV Env immunogens resolved
980 using cryoEM. *Nat Commun* **12**, 4817 (2021).
981 58. Barnes, C.O. et al. Structural characterization of a highly-potent V3-glycan broadly
982 neutralizing antibody bound to natively-glycosylated HIV-1 envelope. *Nat Commun* **9**,
983 1251 (2018).

59. Dong, Y., Tang, H., Dai, H., Zhao, H. & Wang, J. The application of nanodiscs in membrane protein drug discovery & development and drug delivery. *Front Chem* **12**, 1444801 (2024).
60. He, L., Diedrich, J., Chu, Y.Y. & Yates, J.R., 3rd Extracting Accurate Precursor Information for Tandem Mass Spectra by RawConverter. *Anal Chem* **87**, 11361-11367 (2015).
61. Xu, T. et al. ProLuCID: An improved SEQUEST-like algorithm with enhanced sensitivity and specificity. *J Proteomics* **129**, 16-24 (2015).
62. Tabb, D.L., McDonald, W.H. & Yates, J.R., 3rd DTASelect and Contrast: tools for assembling and comparing protein identifications from shotgun proteomics. *J Proteome Res* **1**, 21-26 (2002).
63. Peng, J., Elias, J.E., Thoreen, C.C., Licklider, L.J. & Gygi, S.P. Evaluation of multidimensional chromatography coupled with tandem mass spectrometry (LC/LC-MS/MS) for large-scale protein analysis: the yeast proteome. *J Proteome Res* **2**, 43-50 (2003).
64. Park, S.K., Venable, J.D., Xu, T. & Yates, J.R., 3rd A quantitative analysis software tool for mass spectrometry-based proteomics. *Nat Methods* **5**, 319-322 (2008).
65. Hurtado, J. et al. Efficient isolation of rare B cells using next-generation antigen barcoding. *Front Cell Infect Microbiol* **12**, 962945 (2022).
66. Breden, F. et al. Reproducibility and Reuse of Adaptive Immune Receptor Repertoire Data. *Front Immunol* **8**, 1418 (2017).
67. Punjani, A., Rubinstein, J.L., Fleet, D.J. & Brubaker, M.A. cryoSPARC: algorithms for rapid unsupervised cryo-EM structure determination. *Nat Methods* **14**, 290-296 (2017).
68. Bepler, T. et al. Positive-unlabeled convolutional neural networks for particle picking in cryo-electron micrographs. *Nat Methods* **16**, 1153-1160 (2019).
69. Punjani, A. & Fleet, D.J. 3D variability analysis: Resolving continuous flexibility and discrete heterogeneity from single particle cryo-EM. *J Struct Biol* **213**, 107702 (2021).
70. Punjani, A., Zhang, H. & Fleet, D.J. Non-uniform refinement: adaptive regularization improves single-particle cryo-EM reconstruction. *Nat Methods* **17**, 1214-1221 (2020).
71. Abramson, J. et al. Accurate structure prediction of biomolecular interactions with AlphaFold 3. *Nature* **630**, 493-500 (2024).
72. Pettersen, E.F. et al. UCSF ChimeraX: Structure visualization for researchers, educators, and developers. *Protein Sci* **30**, 70-82 (2021).
73. Casanal, A., Lohkamp, B. & Emsley, P. Current developments in Coot for macromolecular model building of Electron Cryo-microscopy and Crystallographic Data. *Protein Sci* **29**, 1069-1078 (2020).
74. Afonine, P.V. et al. Real-space refinement in PHENIX for cryo-EM and crystallography. *Acta Crystallogr D Struct Biol* **74**, 531-544 (2018).
75. Conway, P., Tyka, M.D., DiMaio, F., Konerding, D.E. & Baker, D. Relaxation of backbone bond geometry improves protein energy landscape modeling. *Protein Sci* **23**, 47-55 (2014).